C.P. No. 960

C.P. No. 960

MINISTRY OF TECHNOLOGY

AERONAUTICAL RESEARCH COUNCIL

CURRENT PAPERS

Free-flight Measurements of the Incremental Drag due to Engine Nacelles on a Transonic Swept-wing Aircraft

by

G. K. Hunt

LONDON: HER MAJESTY'S STATIONERY OFFICE

1967

PRICE NINE SHILLINGS NET

U.D.C. No. 533.6.013.12 : 533.695.9 : 533.695.129 : 533.6.011.35

C.P. No 960
June 1966

FREE-FLIGHT MEASUREMENTS OF THE INCREMENTAL DRAG DUE TO ENGINE NACELLES ON A TRANSONIC SWEPT-WING AIRCRAFT

by

G. K. Hunt

SUMMARY

Models of a swept-wing aircraft, without nacelles and with a pair of simple nacelles attached in three different ways, wore flown at transonic and low supersonic speeds at Reynolds numbers up to 10 million. From measurements of their zero-lift drag the incremental drag caused by each nacelle installation was determined.

A breakdown of the incremental drag shorn that, at the design Mach number of 1·2, the external drag caused by a pair of pylon-mounted nacelles on the wing or on tho body was about twice that caused by a pair of nacelles attached directly to the mng.

Replaces R.A.E. Technical Report 66181 - A.R.C. 28388

CONTENTS

1 INTRODUCTION

About ten years ago the first supersonic transports were foreseen as swept-wing aircraft, which would fly economically at low supersonic speeds by maintaining a shock-free, subsonic type of flow over the wing. As part of the considerable research effort that was directed at that time towards the establishment of design principles for this kind of aircraft, an extensive programme of free-flight tests was undertaken. These tests had three objects: to investigate methods of wing-body junction design, to measure the effect of wing camber and twist on drag due to lift, and to measure the external drag penalties caused by adding engine nacelles to a swept-wing aircraft in various ways.

The first object was achieved and this part of the work is reported in Ref.1. While the remaining tests were getting under way the narrow delta wing emerged as the most promising shape for the first generation of supersonic transport aircraft. Although this caused some swept-wing research to be curtailed the free-flight tests continued, but without their original urgency. The models were tested at an average rate of one flight per year until the work was completed in 1965.

One basic model aircraft configuration was common to all three groups of free-flight tests, and provided a link between the three sets of results. The effect of engine nacelles on the drag of this configuration was investigated by attaching a pair of simple nacelles in three different ways and measuring the resultant drag increments. In this report the drag increments are compared to the drag of two isolated nacelles and are analysed to obtain the Installation Drag[2]; this is the external normal-pressure drag caused by adding the nacelles and any supporting pylons. In order to obtain a satisfactory drag breakdown the internal drag of the basic nacelle was determined separately from a wind-tunnel test.

The results show that, in respect of drag, there is little to choose between pylon-mounted nacelles on the wing or on the rear body, but there is a worthwhile reduction of external drag to be obtained by eliminating the pylons.

2 MODEL DESIGN

2.1 The basic model aircraft

The aircraft configuration to which the nacelles were added consisted of a slender body of revolution, a wing swept back 55 degrees, and a simple tail unit with cropped delta surfaces (Fig.1). The geometry is described in this

report; a fuller account of the evolution of the design and of the method of calculating the body profile is given in Ref.1.

The wing had an aspect ratio of 3·40. The trailing edge was straight from root to tip, with a constant chord over the inboard half of the span and a parabolic leading edge on the outboard half which reduced the chord to zero at the tip. The ordinates are *given in* the Appendix. The aerofoil section was RAE 101, with a uniform thickness/chord ratio of 0·06.

The body was designed by redistributing the volume of on ogive-cylinder-ogive body in accordance with the supersonic area rule. The design Mach number of the whole aircraft was 1·2 but, in order to reduce the risk of a drag peck at sonic speed, tho area-rule calculations were based on a design Mach number of 1·16. It would hove been impossible to fit sufficient telemetry equipment into a fully waisted body without a considerable increase in tho size of tho models. Therefore a partially waisted body was adopted. Its cross-section areas differed from those of the unwaisted body by only 60 per cent of the amounts required by tho area rule. Calculations by Lord, based on those in Ref.3, justified this procedure and tho resultant body proved to be vary effective. At all Mach numbers up to 1·4 the flow in the wing-body junction remained shock-free and the drag remained low'. The ordinates of tho body profile arc given in the Appendix.

2.2 The basic model nacelle

The model nacelle (Fig.2) was based on a proposal to accommodate two engines side by side. It consisted of a conical forebody with a sharp-lipped pitot *intake,* a cylindrical centre-body, and a convergent afterbody tapering *to a* simple, sharp-lipped nozzle. The external surface slopes on the forebody and the-afterbody were the same, and all cross-sections were oval.

The interior of the model was essentially a divergent-convergent duct. The ratio between tho intake and exhaust cross-section areas was calculated so that the boundary-layer growth along the duct would just cause the exhaust nozzle to choke at the highest Mach number of the tests. This was intended to maintain subsonic internal flow, end thus to sustain a realistic intake shock pattern at supersonic speeds, while minimising spillage throughout the range of Mach numbers covered by the tests.

2.3 Nacelle installations

Three different nacelle installations were designed by adding a pair of nacelles to the model sircraft. The nacelles wore attached to tho wing and

to the rear body on pylons, and directly to the wing without pylons. The general arrangement of the three model configurations is shown in Fig.3. The volume of the body was reduced. slightly to compensate for the added volume of the wing-mounted nacelles, but no compensation was made for the nacelles on the rear body.

The nacelles of model A were suspended below the wing on pylons at mid-span (Figs.4 and 5). The pylons had a thickness/chord ratio of *0.04 and were* yawed. 4 degrees to align them approximately with the calculated. direction of the local flow over the wing. They were swept through the same angle as the wing, and their chord was half the length of a nacelle. The distance of the nacelle axes below the plane of the wing was one-fifth of the local chord. The nacelles were placed in front of the wing, to represent a type of installation that has been widely used on subsonic transport aircraft. The longitudinal position of the intakes was chosen so that, at the design Mach number, the intake shocks would intersect the wing-body Junction one-third of the root chord behind the leading edge. This position was one of a series that were to be investigated in a wind tunnel. The tunnel tests were later cancelled.

Model B represented the kind of configuration that would be required to accommodate the engines partly within tha wing behind the main spars. A pair of nacelles was built into the lower surface of the wing at the mid-span position (Figs.4 and 6). Since the wing section had a roof-top chordwise pressure distribution', the intakes were placed where they would avoid the extremes of pressure that occur near the leading edge and would lie within the flat part of the roof-top. Thus the pressure distribution across the intakes should have been approximately uniform. The nacelles extended beyond the trailing edge of the wing. At the exhaust nozzle the oval cross-section of the basic nacelle was retained, but within the chord of the wing the cross-sections were D-shaped. Between the trailing edge and the ends of the nacelles the cross-section shapes changed progressively. As a result, the external area distribution of these nacelles differed slightly from that of the basic nacelle but the internal area distribution of the ducts was not affected.

The boundary layer on the wing of model B was not diverted, and passed into the intakes.

Model C had its nacelles mounted on unswept pylons on each side of the rear body (Figs.4 and 7). This arrangement offers the advantage of a completely clean wing, *and has* already been used successfully on subsonic transport aircraft. The nacelles wore installed with their axes parallel to the body

axis and in tho plane of the wing. The exhaust nozzles were level with the end of the body, and the long axes of the oval cross-sections were normal to the plane of the wing. The clearance between the inboard lips of the intakes and the sides of the body was two-thirds of the calculated thickness of the boundary layer on the body at the design Mach number of 1·2. The pylons, like those of model A, had a chord equal to half the length of a nacelle and a thickness/chord ratio of 0·04.

The bodies of models A and B differed from that of the basic model aircraft because their volumes were reduced to compensate for the added volume of the nacelle installations (Fig.8). Only partial compensation was provided because the basic body had been partially waisted to compensate for the wing volume (see section 2.1). The change of volume was small and the nacelles did not differ very much from bodies of revolution. Therefore the full prooedum required by the supersonic area rule, entailing the calculation of several oblique area distributions, was not followed. Instead the effective area distribution of the nacelles was obtained by assuming that their internal area distribution was linear from intake to exhaust. Then in each case 60 per cent of the effective volume of the complete nacelle installation was removed from the part of the basic body within the Mach diamond enclosing the nacelle installation at the design Mach number of 1·2. The area distribution of the volume removed was sinusoidal. The profile ordinates of both bodies are given in the Appendix.

The body of model C was identical to that of the basic model aircraft. Even partial waisting, of the kind employed in the design of models A and B, would have produced a body that was structurally impracticable.

3 EXPERIMENTAL TECHNIQUE

3.1 Determination of internal drag

To enable the drag of the nacelle installations to be analysed it was necessary to determine their internal drag, but it was impracticable to do so in flight. Instead the internal skin-friction drag was estimated, and the internal normal-pressure drag was derived from pressure measurements made in an isolated nacelle in the R.A.E. 3 ft x 3 ft wind tunnel. This method had the dual advantage that it avoided scale effect and obviated the need for an experimental survey of the internal boundary layer.

To estimate the internal friction drag, the variation of Mach number and Reynolds number along the duct was calculated, taking account of the effect of

the displacement thickness of the internal boundary layer. Then the friction drag was obtained from the curves of Ref.5.

For the wind-tunnel test, a **nacelle** was attached to the end of a sting support by means of a pylon, so that the intake was substantially free from support interference. In a plane $\frac{1}{4}$ inch forward of the rear end of the nacelle, static pressure was measured on the nacelle centre-line and pitot pressure at eleven other points. All the pitot tubes were clear of the internal boundary layer so that they would not detect any loss of momentum due to skin friction.

The wind-tunnel test was completed before the free-flight tests began. As well as providing internal drag measurements it verified the design by demonstrating that the flow inside the nacelle was always subsonic and there was very little spillage. This was regarded as sufficient proof of the pylon-mounted nacelles, and no measurements were made in flight to check the flow through the nacelles of models A and C. However, the nacelles of model B were not mounted on pylons, and the internal flow included the boundary layer on part of the wing. Therefore static pressures were measured in flight in both nacelles of this model, to check whether the flow always remained subsonic and to detect thickening or separation of the internal boundary layer.

3.2 *Free-flight tests*

The weight, centre of gravity position and inertia characteristics of each model were measured before its flight. The moments of inertia, about the body axis and about spanwise and normal axes through the centre of gravity, were measured by suspending the model on two wires of equal length and swinging it as a bifilar pendulum about each axis in turn. Corrections were applied to account for the masses of the wire attachments.

The models were launched from the ground and reached their maximum velocity in about 3 seconds. They all achieved maximum Mach numbers close to 1·45 (Fig.9) and maximum Reynolds numbers, based on $\bar{c}$, of about 10 million (Fig.10). The booster rockets (Fig.4) were dotnched as soon as they stopped thrusting, and the experimental measurements were made while the models were decelerating in free flight. Boundary-layer transition was allowed to occur naturally. In order to trim the models as nearly as possible at zero lift throughout their flights, their tailplanes were fixed at a small positive angle relative to the body axes. This angle was determined from wind-tunnel tests and from measurements of the flight behaviour of the models described in Ref.1.

Every model carried standard R.A.E. 465 Mc/s telemetry equipment to provide measurements of acceleration and, in the case of model B, of pressure.

Normal and lateral accelerations were measured at the centre of gravity to indicate trim, and at positions near the nose and tail so that stability could be investigated if necessary. Two accelerometers were installed in each model to provide independent measurements of longitudinal deceleration. Static pressure was measured at six points in each nacelle of model B. Ambient pressure and local static temperature were determined separately from radiosonde measurements.

The flight path coordinates and velocity of each model were determined from measurements made by synchronised kinetheodolites at several stations along the range. Additional measurements of velocity were obtained by means of a radio-Doppler transponder carried in the model. Since the velocity measurements could be differentiated to obtain longitudinal deceleration there were effectively four sources of information on the drag of the model. They were not entirely independent, because the airborne accelerometers shared a common transmitter and the calculation of drag always depended on the kinetheodolite measurements of altitude and flight-path direction. Nevertheless the redundancy of information allowed doubtful measurements to be rejected and provided some insurance against failure of the airborne instrumentation. In the event there were no failures, and all the drag measurements were obtained from the accelerometers.

3.3 Analysis and presentation of results

The points in the nacelles of model B at which static pressure was measured in flight are shown in Fig.11. These measurements were reduced to pressure coefficients and are plotted in Fig.12. To obtain some indication of the extent of the potential flow through each duct at supersonic speeds, the ratio between the pressures measured at the maximum cross-section and the exhaust nozzle was used to calculate the corresponding effective cross-section area ratio, assuming a choked nozzle and one-dimensional potential flow. The effective area ratios are plotted in Fig.13.

The internal drag of the ducts was expressed in the form of Standard Internal Drag. This is defined[6] by the equation

$$C_{D_{SN}} = \frac{1}{qS}\left\{mV_\infty - \int \rho_e V_e dA_e - \int (p_e - p_\infty)\, dA_e\right\}.$$

The first two terms on the right-hand side describe the momentum lost per second by the air flowing through the ducts, between a station far ahead of the intakes and the exhaust nozzles. This includes the estimated loss due to

skin friction and the loss, measured in the wind tunnel, due to the distribution of normal pressure on the duct walls and on the pre-entry stream tubes. The third term is the thrust due to the difference of static pressure between the exhaust and the free stream. The internal drag of One isolated nacelle is plotted in this form in Fig.14(a), showing the estimated contribution due to skin friction. (The coefficient of internal skin-friction drag fell rather rapidly with increasing flight Mach number because the mean internal Mach number remained almost constant.) For the purpose of analysing the flight measurements, the Standard Internal Drag of all the nacelle installations was assumed to be twice that of the isolated nacelle.

In order to provide a datum to which the installed drag of the nacelles could be referred, the total drag of en isolated nacelle was found by estimating its external drag and adding it to the Standard Internal Drag. The external skin-friction drag was obtained by using the curves of Ref.7, assuming flat-plate flow with zero heat transfer and a transition Reynolds number of 2 million. The wave drag was obtained by treating the nacelle as a body with elliptic cross-sections and the same external area distribution, and using the curves of Refs.8 and 9. The interference effect of the forebody on the afterbody was taken into account, but spillage drag was neglected. The external drag is plotted in Fig.14(b).

The free-flight tests provided measurements of the total drag of each model (Fig.15). Before the drag was determined, the accelerations indicated by the two longitudinal accelerometers in each model were integrated and the resultant velocities compared with those calculated from the kinetheodolite records. The data from the accelerometer that yielded the closest agreement with the kinethcodolite velocities throughout the flight were used to obtain the drag of the model.

The drag increment caused by each nacelle installation was obtained by subtracting the drag of the basic model aircraft from the drag of the model with nacelles. The increments obtained from all three installations are plotted together in Fig.16. It is helpful to express the drag increment as a multiple of the drag of two isolated nacelles, and this is done in Fig.17. Then the total dreg of a complete configuration is simply given by

$$C_{D_{AN}} = C_{D_{AO}} + K_N C_{D_{NO}} .$$

Each increment of total drag was analysed by subtracting the Standard Internal Drag to obtain the external drag increment, and by subtracting from that the estimated external skin-friction drag increment (Fig.18). The remainder is

the external normal-pressure drag increment; as suggested by Bratton[2] this is called the Installation Drag (Fig.19). Thus an alternative expression for the total drag of a complete configuration is

$$C_{D_{AN}} = C_{D_{AO}} + (C_{D_{SN}} + C_{D_{FN}} + C_{D_I})$$

The drag analysis is summarised in Fig.20 and Table 4. It is confined to supersonic speeds because no measurements of the drag of the basic model aircraft were obtained at subsonic speeds.

The installation drag includes contributions caused by spillage from the intakes and by the influence of the nacelle wakes on the flow around the rear of the aircraft. Both are likely to be small because, in these tests, the spillage was deliberately minimised and the nacelle wakes were either some distance outboard of the body and tail or were shed from the extreme rear of the aircraft.

Finally, the total drag measurements are compared with those obtained[10] under similar free-flight test conditions from an M-wing model (Fig.21). This was derived from the basic swept-wing model, and had the same gross wing area and the same tail unit. Its body was based on the same ogive-cylinder-ogive as the bodies of the swept-wing models, but it was not designed by means of the area rule. The sides of the body were waisted in the region of the wing root, to produce a sheared-wing velocity distribution in the wing-body junction. Waisted closed bodies were installed at the mid-span kinks, and there was a cone-cylinder fairing under the tail that was not fitted to any of the swept-wing models. The drag comparison is made in Fig.22.

3.4 Uncertainty of results

The ambient conditions were determined with negligible error. The uncertainty in the velocity measurements arose almost entirely from the correction for wind velocity, and was about ±10 ft/sec. The resultant uncertainty in Mach number was therefore about ±0·01 and in the kinetic pressure $\frac{1}{2}\gamma p_s M^2$ about ±1 per cent.

The uncertainty in the flight measurements of drag varied with Mach number. The accelerometers measuring longitudinal deceleration had an uncertainty of measurement of ±0·03g. The deceleration of the models varied from about 2·5g at M = 1·4 to about 1·2g at sonic speed, and fell to about 0·5g at subsonic speeds. Thus the uncertainty in the drag coefficients obtained from the flight measurements ranged from about ±1½ per cent at

M=1·4 to about ±2½ per cent at M = 1. It rosa to more than ±6 per cent at subsonic speeds, but this was unimportant because the drag analysis was confined to supersonic speeds.

Slight uncertainty was introduced by the simplicity of the analysis. The internal drag was always assumed to bo twice that of an isolated nacelle, whereas the nacelles on the free-flight models were in different Darts of tha flow field around the aircraft. All the nacelles were behind the shock generated by the nose at supersonic speeds. In addition, part of the wing boundary layer passed through the nacelles of model B and port of the wing wake through those of model C. The effects on the internal drag could not have been measured in flight, and no attempt has been made to estimate them. Since the internal flow contributed only a small part of the total drag, the differences of internal drag would have had to be about 50 per cent to be comparable with the uncertainty of the flight measurements. In calculating the uncertainties of the installed drag factor K_N and of the Installation Drag an uncertainty of ±10 per cent in the Standard Internal Drag was assumed.

The uncertainty of the estimated external skin friction drag on a nacelle installation was about ±3 per cent. Since this was a small component of the total drag its effect was dominated by the uncertainty of the flight measurements.

Since linear theory is reliable as long as its assumptions remain valid, the uncertainty of the estimated wave drag was assumed to be zero. The uncertainty of the installed drag factor K_N then varied from about ±5 per cent at M = 1 to about ±3½ per cent at M = 1·4. If the linear-theory assumptions were violated, perhaps because finite disturbances occurred where surface slopes changed rapidly, then the estimated wave drag of an isolated nacelle may be in error. However, its uncertainty would have to be ±30 per cent to double the uncertainty of K_N.

Most of the uncertainty in the Installation Drag occurred because it was obtained by analysing the difference between two large forces measured in flight. Over the range of supersonic speeds covered by the analysis it was an almost linear function of Mach number. The estimated uncertainties are summarised in the following table.

Table 1

Uncertainty of installation drag

	M = 1	M = 1·4
Uncertainty in C_{D_T}	±0·00080	±0·00049
Uncertainty (Models A & C per cent (Model B	±25 ±67	±15 ±20

4 DISCUSSION OF RESULTS

The pressures measured in the nacelles of model B (Fig.12) give a reassuring picture of the flow through the ducts in flight. The intake pressures show some rearward movement of the intake shocks with increasing Mach number, but they indicate that the shocks moved only a very short distance inside the intakes. This evidence is supported by the high pressures that were always measured at the maximum cross-sections of the ducts. Under the conditions of this test *such pressures could have occurred only while the* flow through the ducts was subsonic.

The exhaust *pressure* measurements, taken at two points in each nozzle, differed somewhat between themselves but all varied in the same way with Mach number. In particular they were all close to free-stream pressure at sonic speed, and increased continuously with *mm-easing* Mach number at supersonic speeds. This suggests that the nozzles were choked, although the measured pressures at supersonic speeds were lower than would. be necessary to obtain an isentropic expansion to free-stream conditions downstream of the nozzles. The *differences* between *the measured* exhaust pressures almost certainly occurred because of a local irregularity in the surface of the starboard duct.

The effective area ratios, calculated from the *measured* pressure ratios, do not agree with each other very well (Fig.13) but none of them differs from the area ratio of the ducts sufficiently to suggest separation or excessive thickening of the internal boundary layer. Thus the passage through the ducts of part of the boundary layer on the wing did not have an adverse effect on the internal flow.

The curves of total *drag* coefficient against Mach number are generally similar in shape (Fig.15). There is a distinct minimum near $M = 1{\cdot}2$ in the curves for the two models which had their bodies redesigned to compensate for the added volume of the nacelle installations, but this may be fortuitous.

The increments of total drag caused by the pylon-mounted nacelle installations of models A and C were nearly the same (Fig.16). The drag increment caused by the nacelles of model B was much lower and, at Mach numbers up to 1·2, was scarcely more than half that caused by the other installations. When the drag increments are compared to the drag of two isolated nacelles (Fig.17) the pylon-mounted installations are shown to have been reasonably successful. At Mach numbers up to 1·3 the drag increments caused by the nacelle installations of models A and C were less than 50 per cent higher than the drag of two isolated nacelles. However, the drag

increment caused by the nacelles of model B was about 20 per cent below the drag of two isolated nacelles at Mach numbers up to 1·2, and only slightly above it at higher Mach numbers. This shows very clearly the advantage gained by eliminating the pylons. It must be emphasised that the nacelles were not designed to produce favourable wing-nacelle interference. There is little doubt that suitable improvement to the external shape of the nacelles could reduce their installed drag still further, especially on model B.

A full-scale aircraft of this kind would cruise above the tropopause and its linear dimensions would be about 30 times those of the free-flight models. Thus it would operate at Reynolds numbers about 10 times greater than those achieved by the models. Hence the proportion of the total drag contributed by skin friction would be less for the aircraft than for the models. Therefore the total drag increments caused by the nacelle installations would be slightly larger multiples of the drag of two isolated nacelles. Nevertheless, at any given scale the nacelle installation of model B will always have an advantage over the others because of its smaller exposed surface area. This is illustrated by Fig.18, where the skin-friction drag increment caused by the nacelles of model B is shown to be about half that caused by the other installations.

The curves of installation drag (Fig.19) reflect the variation of total drag increment with Mach number. They are all rather wavy, but this may be misleading because the amplitudes of the waves are generally less than the experimental uncertainty. The installation drags of both the pylon-mounted nacelle installations were approximately the same, and were roughly constant. The installation drag of the nacelles of model B increased with increasing Mach number, but it was only about half that of the other installations at the design Mach number of 1·2. Thus the benefits of eliminating the pylons were not confined to the skin-friction drag.

All the swept-wing models had considerably less drag than the M-wing model (Fig.22). At supersonic speeds the drag of models A and C was roughly 7 per cent lower, and that of model B about 15 per cent lower. Since the bodies at the mid-span kinks of the M wing were not suspended on pylons, the most appropriate comparison is between the M-wing model and model B. No doubt the drag of all the model configurations could be reduced by careful detail design. The improvements would be largely confined to the wing and body of the M-wing configuration since the bodies at the mid-span kinks were originally designed to produce favourable interference and probably cannot be improved a great deal. On the other hand all the swept-wing nacelle installations could probably be *improved* considerably. Thus it is likely to be difficult to reduce

the drag of the M-wing configuration to that of a swept-wing configuration based on model B. A more satisfactory drag comparison would have been obtained if the M-wing model had carried ducted bodies at the mid-span kinks and had not had a bulge under its tail. However, simple calculations suggest that these differences would not have altered tie total drag of the model very much. The external drag would have been reduced by removing the fairing under the tail and by replacing tho closed bodies by ducted bodies, but internal drag would have been added. The total drag would probably have been one or two per cent lower, and this is not enough to affect tho foregoing argument.

5 CONCLUSIONS

The external drag penalties, caused at low supersonic speeds by three different nacelle installations on a swept-wing aircraft, have been determined by means of free-flight tests. The nacelles were attached to the wing and the rear body on pylons, end directly to tho wing without pylons.

The measurements show that, at tho design Mach number of 1·2, tho nacelles attached directly to tho wing caused about half as much external normal-pressure drag, and about half as much external skin-friction drag, as either of tho pylon-mount& nacelle installations. Thus a worthwhile improvement in external drag was obtained by eliminating the pylons.

At Mach numbers up to 1·3 tho pylon-mounted nacelle installations caused drag increments that were loss than 50 por cent greater than tho drag of two isolated nacelles. However, the nacelles attached directly to the wing were particularly successful, because they caused a drag increment that was below tho drag of two isolated nacelles at Mach numbers up to 1·2 and only slightly above it at higher Mach numbers. Since the nacelles were not designed specifically to produce favourable wing-nacelle interference, the drag increments caused by all tho nacelle installations could probably be reduced considerably by suitable detail design.

All tho swept-wing models had loss drag than an M-wing model with the same gross wing area. In particular, tho drag of the model with nacelles attached directly to tho wing was about 15 per cent below that of tho M-wing model.

Appendix

MODEL GEOMETRY

The wing planform was defined as follows. The trailing edge was straight from root to tip and was swept back 55°. The inboard half of the wing had a constant chord and the spanwise distribution of chord over the outboard half of the wing was defined by

$$c = 2c_o \left\{ \left[2\left(1 - \frac{y}{s}\right)\right]^{\frac{1}{2}} - \left(1 - \frac{y}{s}\right)\right\}$$

where

$$0{\cdot}5 \leq \frac{y}{s} \leq 1{\cdot}0 \quad .$$

Chords of the models, calculated by means of this expression, are given in the following table.

Table 2

Ordinates of outboard half of wing planform

Y inches	$\frac{y}{s}$	$\frac{c}{2c_o}$	c inches
9·739	0·50	0·50	12·500
10·0	0·5134	0·4999	12·498
10·5	0·5390	0·4992	12.480
11·0	0·5647	0·4977	12·443
11·5	0·5904	0·4955	12·388
12·0	0·6161	0·4924	12·310
12·5	0·6417	0·4882	12·205
13·0	0·6674	0·4830	12'075
13.5	0·6931	0·4766	11·915
14·0	0.7188	0·4687	11·718
14·5	0·7444	0·4594	11·485
15·0	0·7701	0·4482	ii·205
15·5	0·7958	0·4349	10·873
16·0	0·8214	0·4191	10·478
16·5	0.8471	0·4001	10·003
17·0	0·8728	0·3772	9·430
17·5	0·8985	0·3491	8·728
17·75	0·9113	0.3326	8·315
18·0	0.9241	0·3137	7·843
18·25	0·9370	0·2920	7·300
18·5	0.9498	0·2667	6·668
18·75	0·9626	0·2361	5'903
19·0	0·9755	0·1969	4·923
19·125	0·9818	0·1 724	4'310
19·25	0·9883	0·1413	3·533
19·375	0·9947	0·0981	2.453
19·479	1·0	0	0

The wing section was R.A.E.101, with a thickness/chord ratio of 0·06. Ordinates of this section are given in Ref.4.

All the models had bodies of revolution, designed by a method based on the supersonic area rule. In the following table the body ordinates of models A and B are listed only where they differed from those of the basic model aircraft.

Table 3

Body ordinates

Inches from nose	Body radius (inches)		
	Basic aircraft and model C	Model A	Model B
0	0		
1	0·288		
2	0·486		
3	0·659		
4	0·816		
5	0·960		
6	1·093		
7	1·216		
8	1·331		
9	1·439		
10	1·540		
11	1·635		
12	1·725		
13	1·810		
14	1·890		
15	1·966		
16	2·038		
17	2·107		
18	2'172		
19	2·234		
20	2·292		
21	2·347		
22	2·399		
23	2·448		
24	2·496		
25	2·538		
26	2·579		
27	2·616		
28	2.650	2·648	
29	2·679	2·673	
30	2·703	2·690	
31	2·719	2·695	
32	2·724	2·686	
33	2·710	2·656	
34	2·678	2·607	
35	2.631	2·542	
36	2·573	2·466	
37	2.512	2·388	
38	2·457	2·319	
39	2·411	2'263	
40	2·375	2.220	2·374

Inches from	Body radius (inches)		
	Basic aircraft and model C	Model A	Model B
41	2·349	2.192	2·342
42	2·332	2·177	2·317
43	2·323	2·176	2·296
44	2'319	2·184	2·279
45	2·319	2.199	2·264
46	2·321	2·218	2·249
47	2·323	2.239	2·235
48	2·325	2.260	2·221
49	2.326	2·279	2·209
50	2·326	2·295	2·198
51	2·324	2·306	2·188
52	2·320	2'312	2·179
53	2·312	2·310	2·170
54	2·301		2·162
55	2·286		2·153
56	2·266		2·143
57	2·242		2'131
58	2·21j		2·117
59	2·179		2·099
60	2'141		2·077
61	2.098		2·050
62	2·051		2·018
63	1·999		1·979
64	1·943		1·933
65	1·883		1·880
66	1·819		
67	1·751		
68	1·679		
69	1·604		
70	1·525		
71	1·443		
72	1·356		
73	1·264		
74	1·165		
75	1·058		
76	0·940		
77	0·815		
78	0·690		
79	0.573		
80	0.500		

Table 4

Summary of drag analysis

Mach number		1.05	1.10	1.15	1.20	1.25	1.30	1.35	1.40
Basic aircraft:	$C_{D_{AO}}$	0.0203	0.0203	0.0202	0.0199	0.0200	0.0206	0.0208	0.0205
Two isolated nacelles	$C_{D_{NO}}$	0.00385	0.00367	0.00359	0.00353	0.00352	0.00351	0.00350	0.00349
	$C_{D_{SN}}$	0.00030	0.00083	0.00087	0.00091	0.00097	0.0010:	0.00107	0.00112
Model A	$C_{D_{AN}}$	0.0261	0.0258	0.0256	0.0255	0.0255	0.0263	0.0270	0.0277
	$C_{D_{AN}} - C_{D_{AO}}$	0.0058	0.0055	0.0054	0.0056	0.0055	0.0057	0.0062	0.0069
	$C_{D_{FN}}$	0.00147	0.00146	0.00145	0.00144	0.00143	0.00141	0.00140	0.00139
	C_{D_I}	0.0035	0.0032	0.0030	0.0033	0.0031	0.0033	0.0037	0.0044
Model B	$C_{D_{AN}}$	0.0232	0.0232	0.0232	0.0235	0.0239	0.0247	0.0249	0.0260
	$C_{D_{AN}} - C_{D_{AO}}$	0.0029	0.0029	0.0029	0.0036	0.0039	0.0041	0.0041	0.0052
	$C_{D_{FN}}$	0.00077	0.00076	0.00075	0.00074	0.00073	0.00072	0.00071	0.00070
	C_{D_I}	0.0013	0.0013	0.0013	0.0020	0.0022	0.0024	0.0023	0.0034
Model C	$C_{D_{AN}}$	0.0260	0.0254	0.0251	0.0252	0.0254	0.0258	0.0263	0.0268
	$C_{D_{AN}} - C_{D_{AO}}$	0.0057	0.0051	0.0049	0.0053	0.0054	0.0052	0.0055	0.0060
	$C_{D_{FN}}$	0.00137	0.00136	0.00135	0.00133	0.00132	0.00131	0.00130	0.00129
	C_{D_I}	0.0035	0.0029	0.0026	0.0031	0.0031	0.0029	0.0031	0.0036

SYMBOLS

A	cross-section area of duct
C_D	drag coefficient, $= D/qS$
C_p	pressure coefficient, $= (p - p_s)/q$
D	drag force
g	acceleration due to gravity
K_N	incremental drag factor, $= (C_{D_{AN}} - C_{D_{AO}})/C_{D_{NO}}$
m	internal mass flow rate
M	Mach number
p	static pressure
p_s	ambient pressure
q	kinetic pressure, $= \frac{1}{2} \gamma p_s M^2$
S	gross wing area
$S(x)$	cross-section area at station x
V	velocity
x	distance along body axis measured rearward from nose
γ	ratio of specific heats of air, $= 1.4$
ρ	air density

Suffixes identifying stations in the internal flow

e	nacelle exhaust
∞	far ahead of the intake

Suffixes identifying drag coefficients

AN	total drag of the model aircraft with nacelles
AO	total drag of the basic model aircraft without nacelles
FN	additional external skin-friction drag caused by nacelle installation
I	Installation Drag, i.e. the additional external normal-pressure drag caused by nacelle installation
NO	Total drag of isolated nacelles
SN	Standard Internal Drag

REFERENCES

NO.	Author	Title, etc.
1	G. K. Hunt	A free-flight investigation of wing-body junction design for a transonic swept-wing aircraft. A.R.C. C.P.759, August 1963
2	J. W. Britton	Measurement of the internal drag of air breathing installations on slender wing-body combinations at supersonic speeds. A.R.C. C.P.914, December 1965
3	W. T. Lord	On the design of wing-body combinations of low zero-lift drag rise at transonic speeds. A.R.C. R & M No.3279, October 1959
4	R. C. Pankhurst H. B. Squire	Calculated pressure distributions for the R.A.E.100-104aerofoil sections. A.R.C. C.P.80, March 1950
5	K. G. Smith	Methods and charts for estimating skin friction drag in mind tunnel tests with zero heat transfer. A.R.C. C.P.824, August 1964
6	ARC Definitions Panel	Definitions of the thrust of a jet engine and of the internal drag of a ducted body. A.R.C. C.P.190, May 1954
7	R.Ae.S.	Aerodynamics data sheets
8	L. E. Fraenkel	The theoretical wave drag of some bodies of revolution. A.R.C. R & M No.2842, May 1951
9	L. E. Fraenkel	Supersonic flow past slender bodies of elliptic cross-section. A.R.C. R & M No.2954, May 1952
10	J. B. W. Edwards	Free-flight measurements of the drag ad longitudinal stability of a transonic M-wing aircraft. A.R.C. C.P.773, November 1963

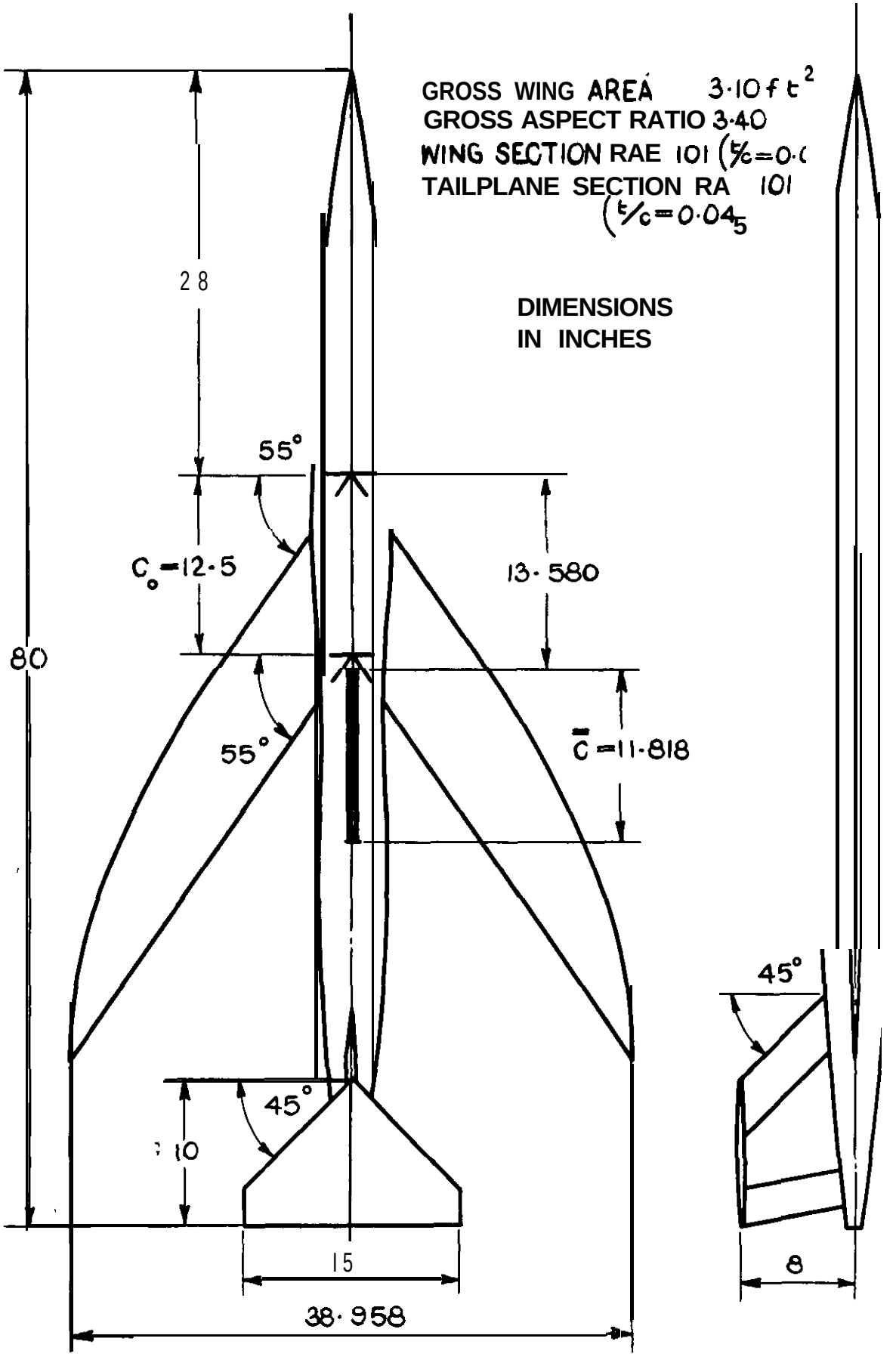

FIG. I THE BASIC MODEL AIRCRAFT

DIMENSIONS IN INCHES

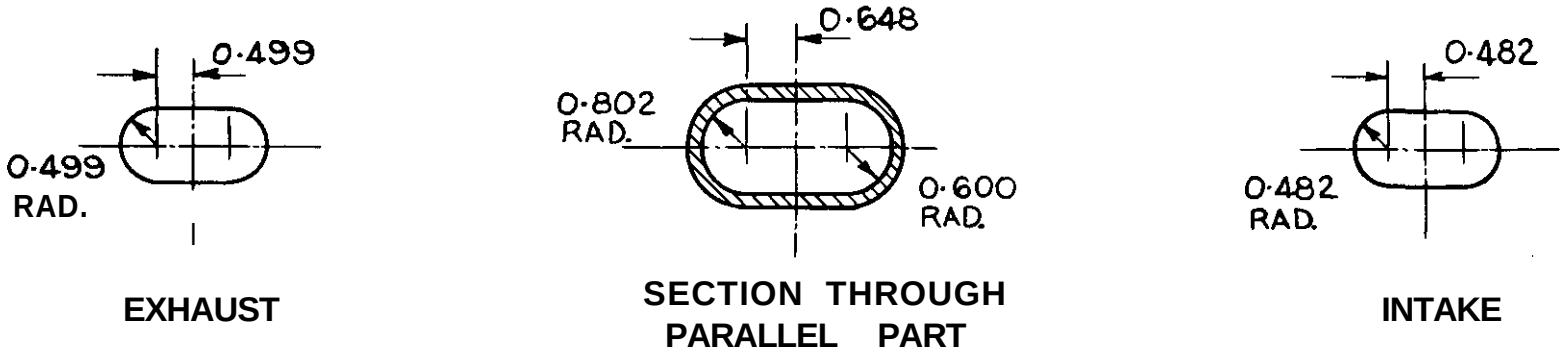

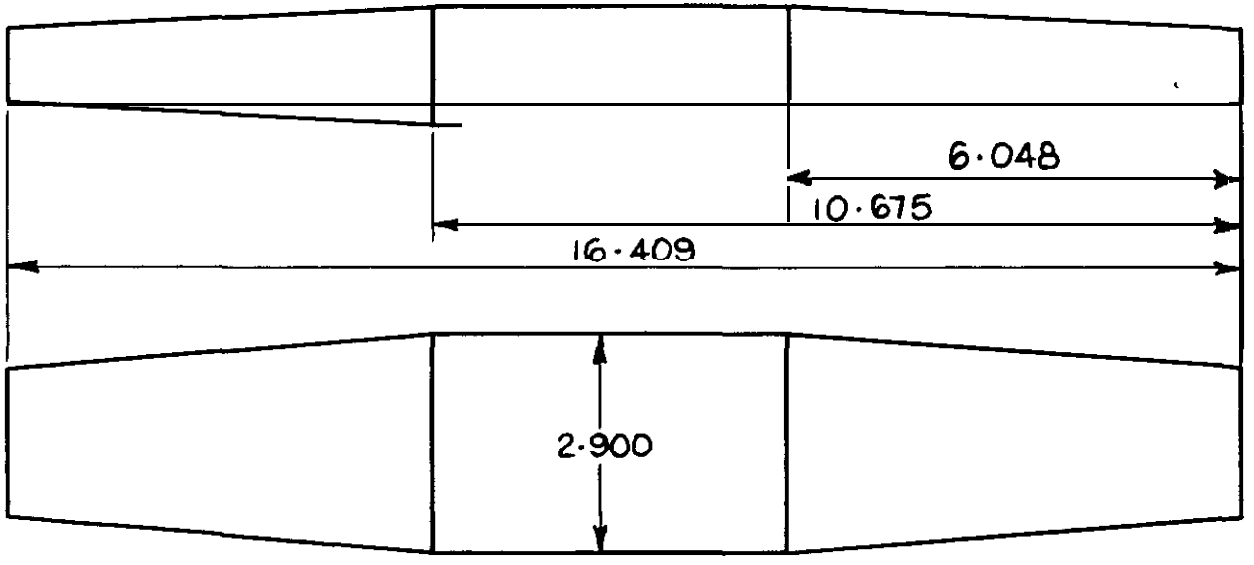

FIG. 2 THE BASIC MODEL NACELLE

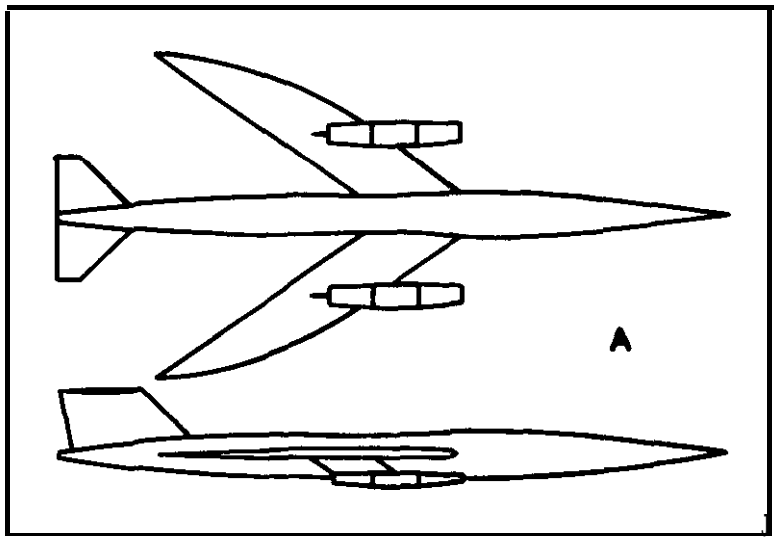

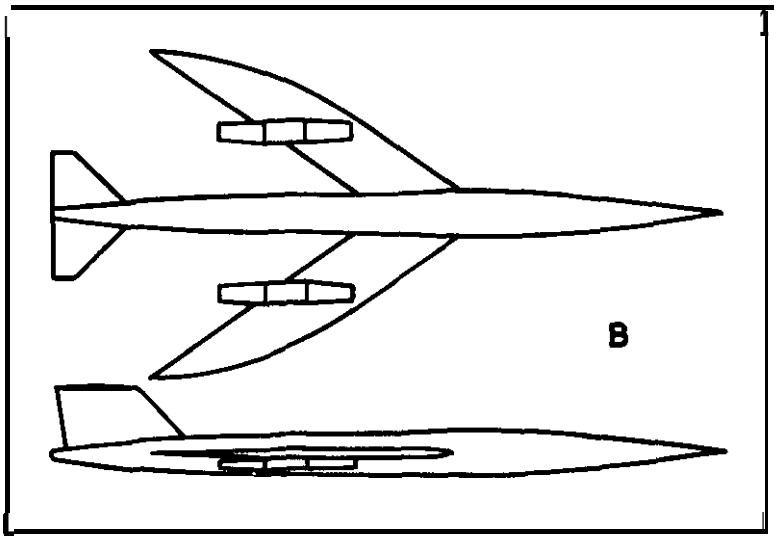

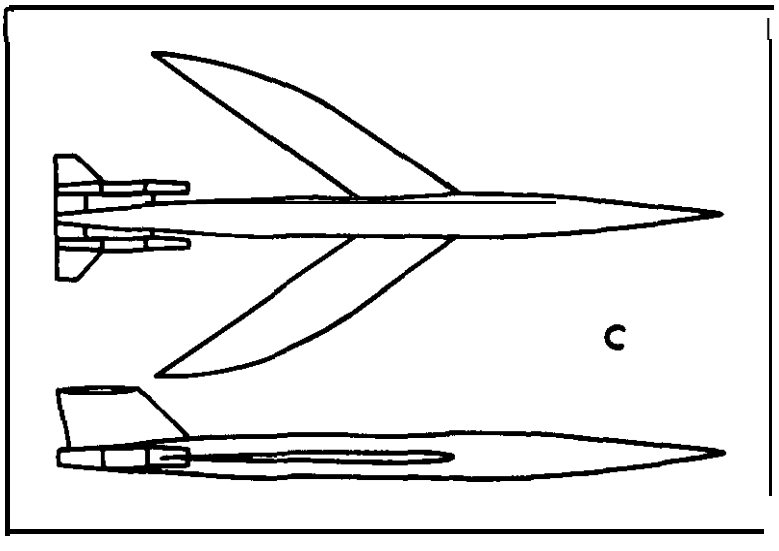

FIG. 3 GENERAL ARRANGEMENT OF THE MODELS

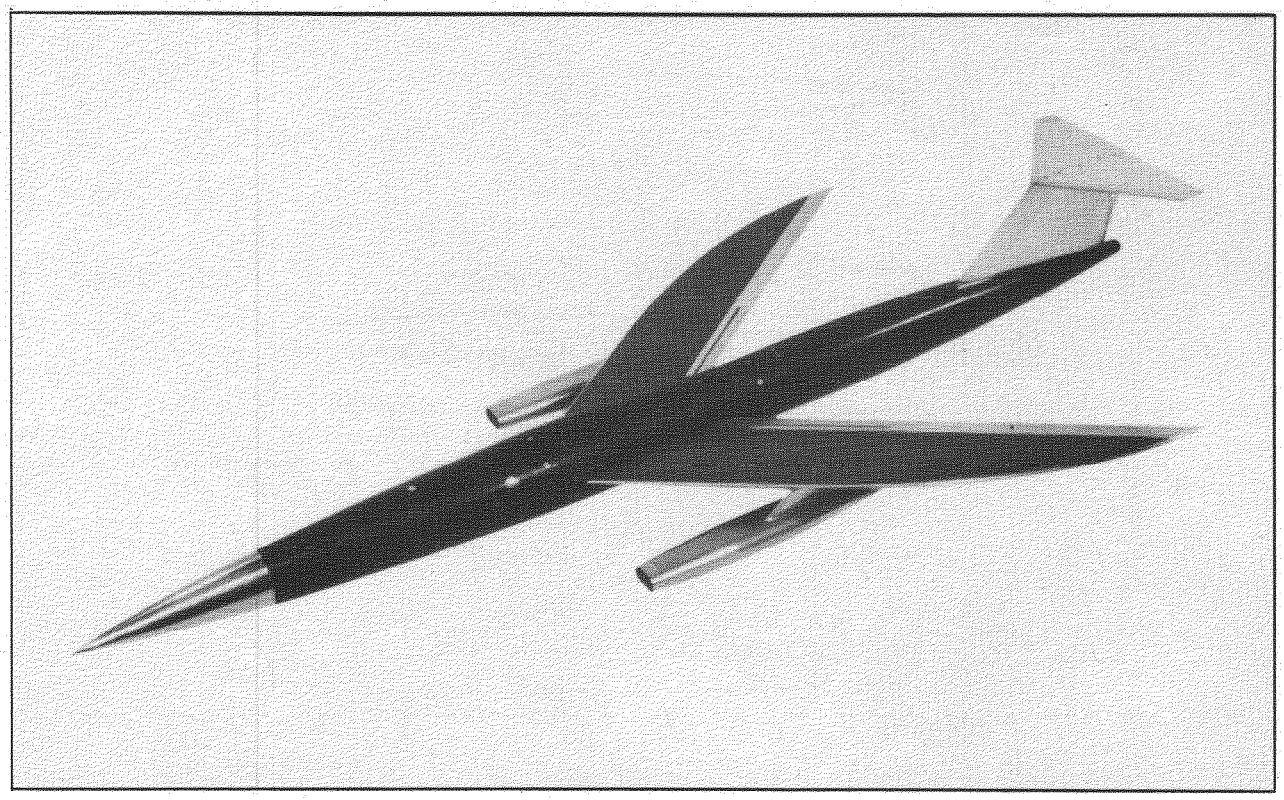

Model A

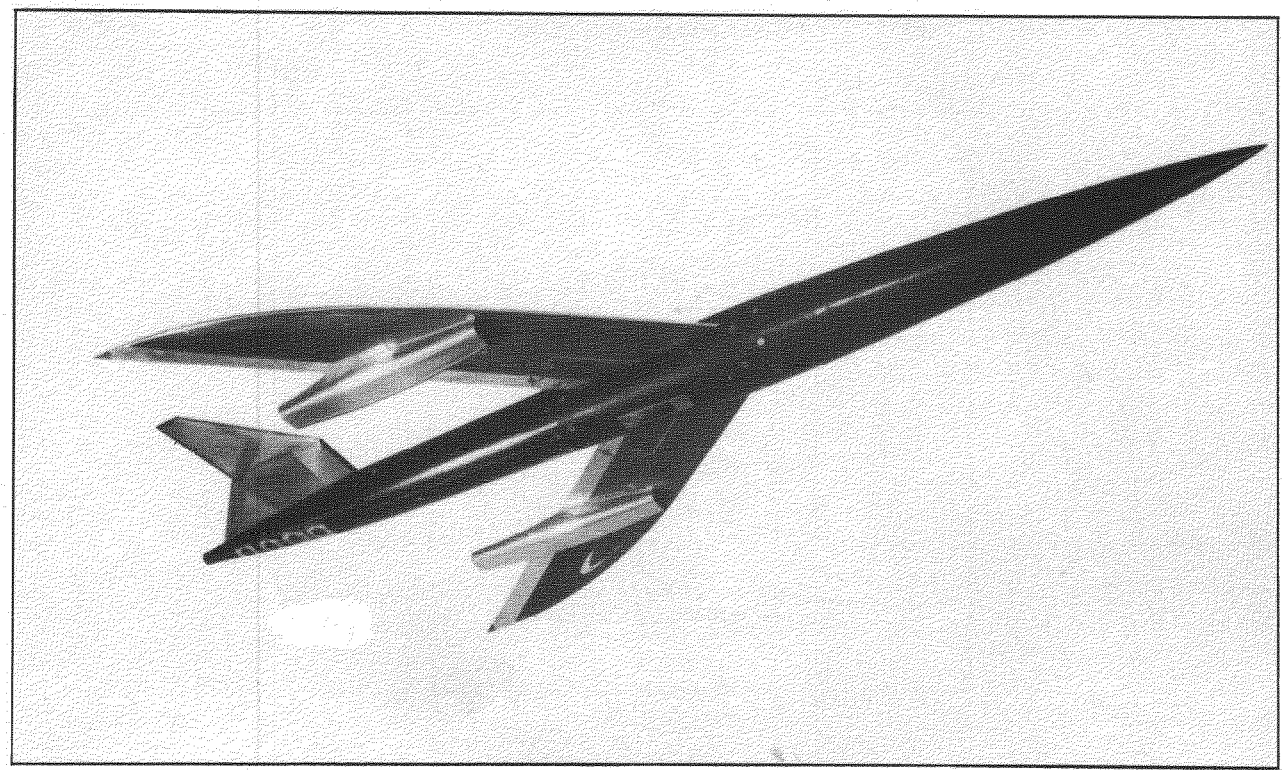

Model B

Fig.4. Photographs of the models

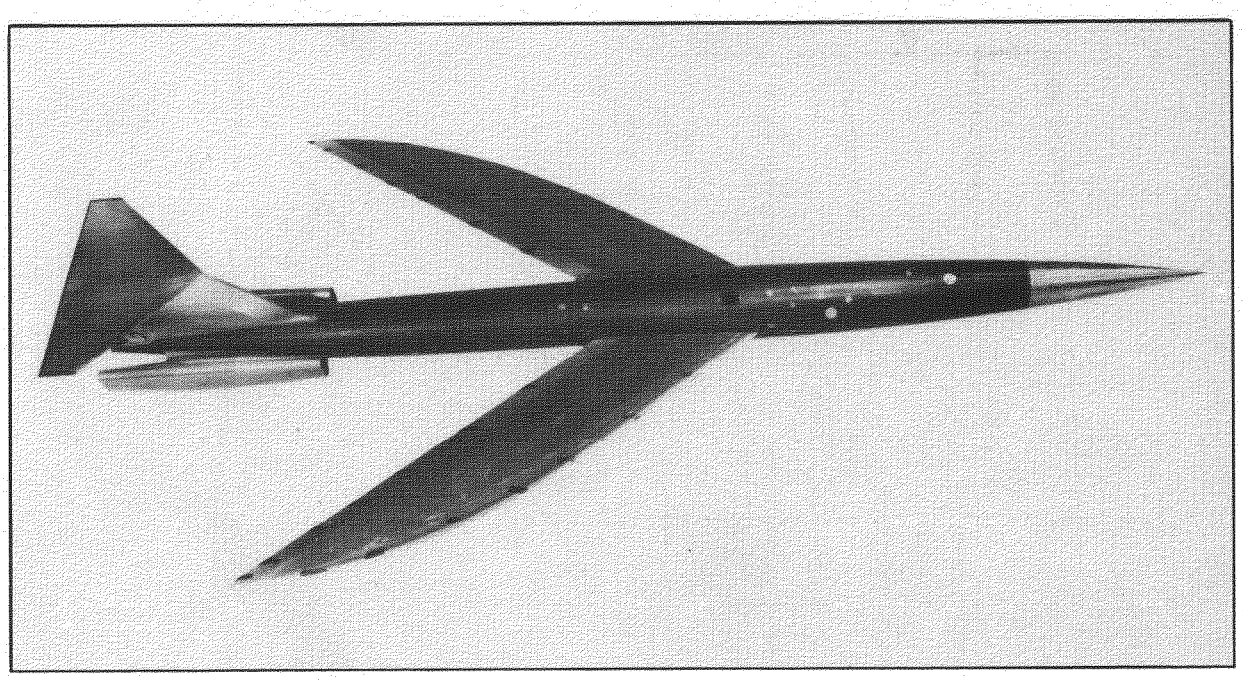

Model C

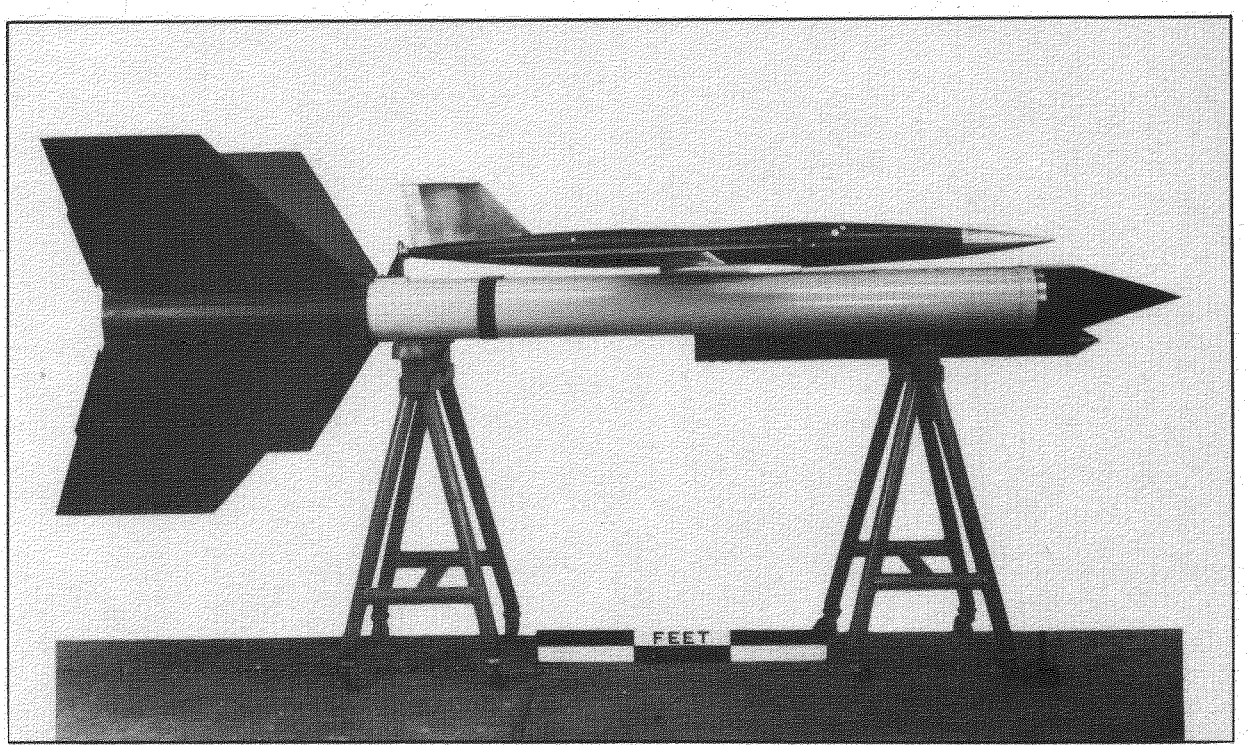

Model A with booster rockets attached

Fig.4 (cont'd). Photographs of the models

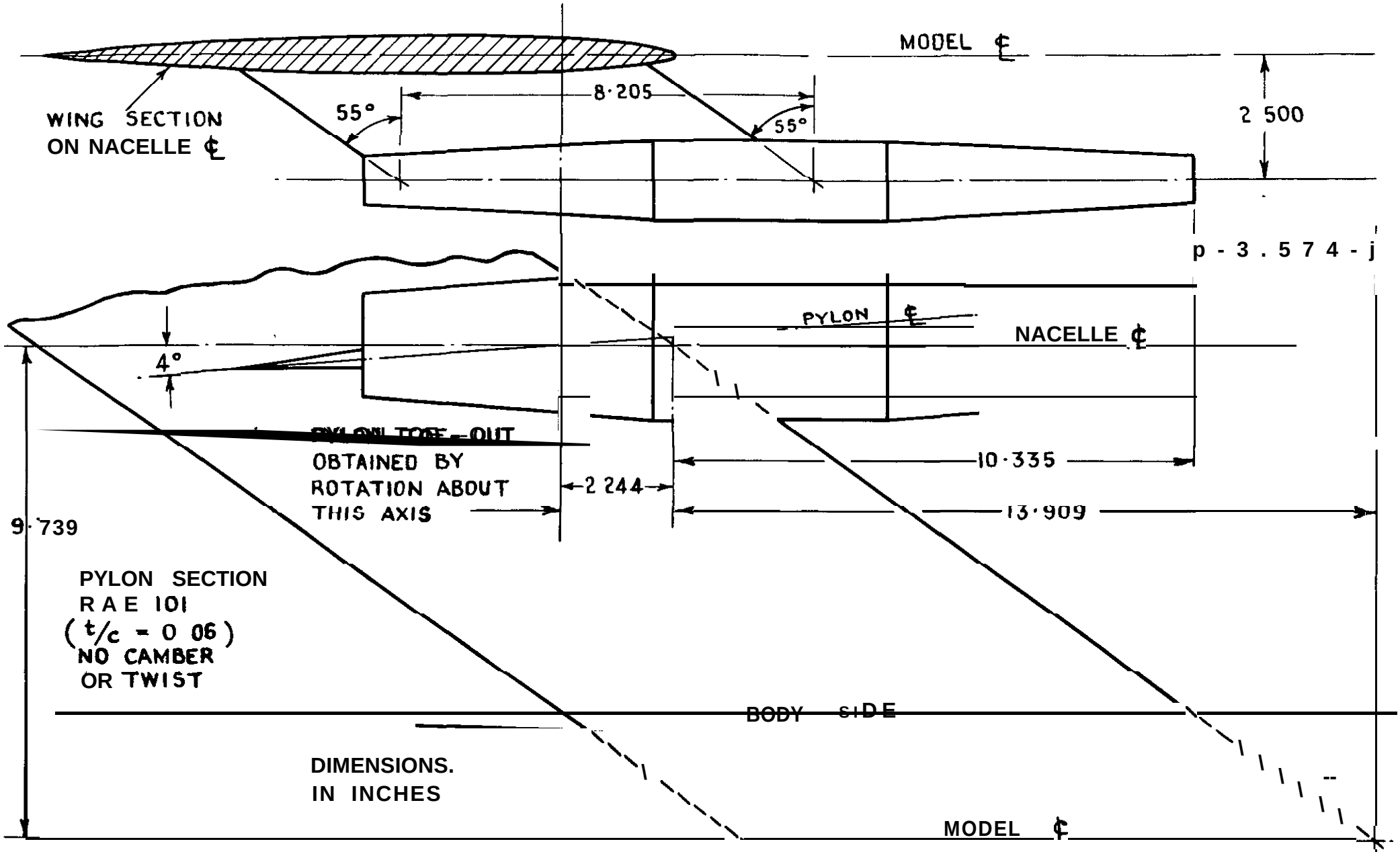

FIG. 5 DETAIL OF MODEL A

DIMENSIONS IN INCHES

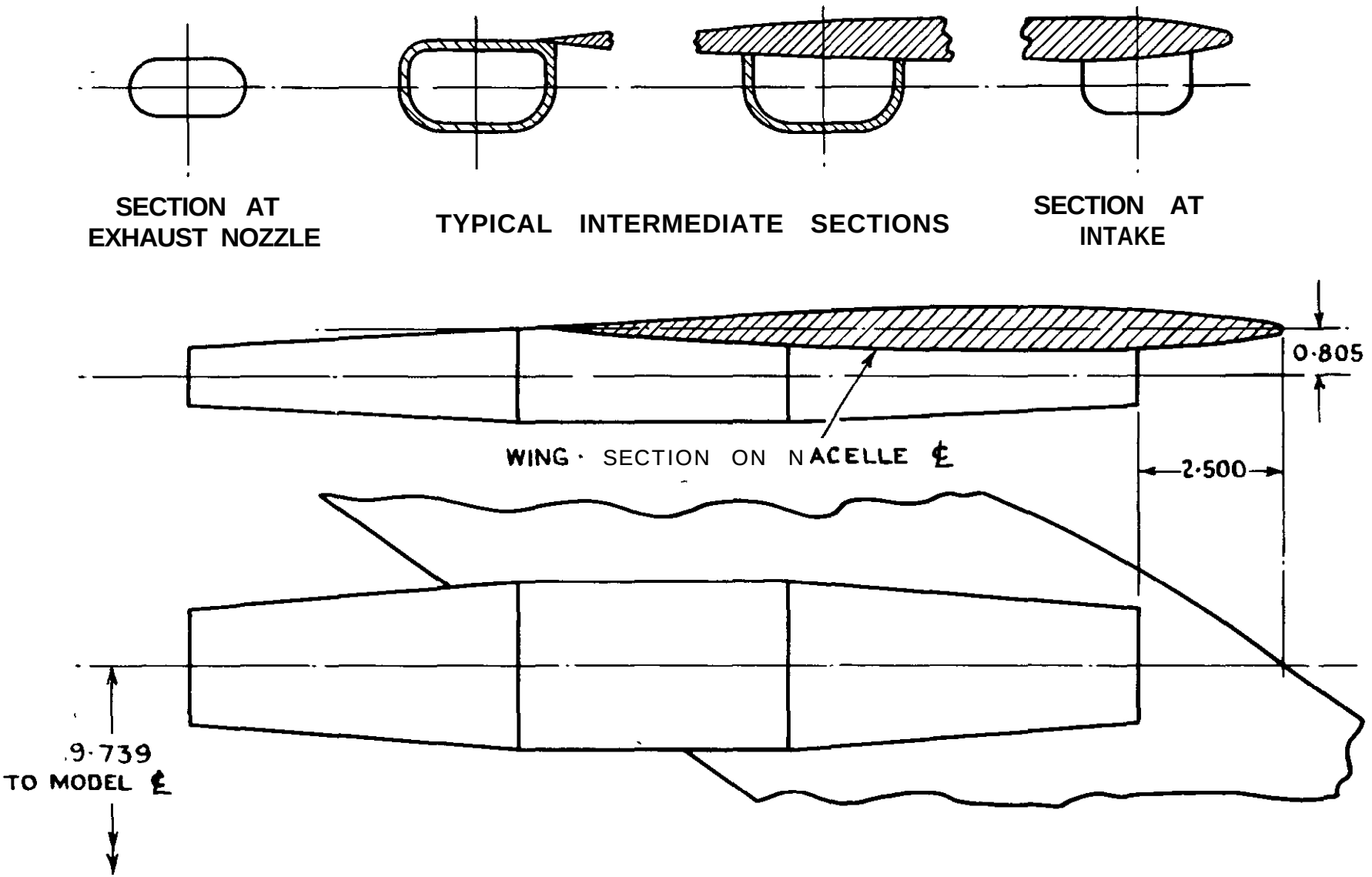

FIG.6 DETAIL OF MODEL B

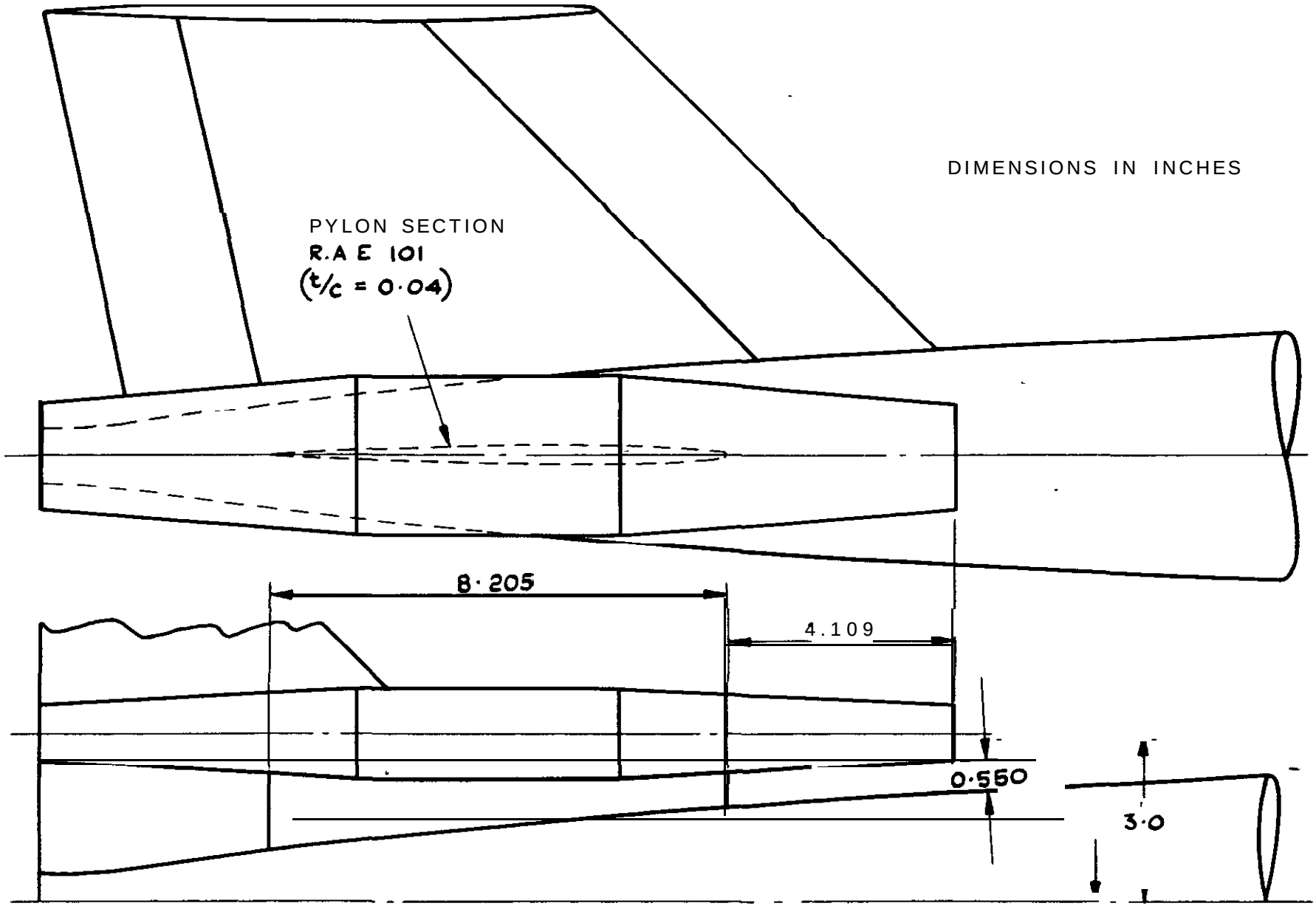

FIG 7 DETAIL OF MODEL C

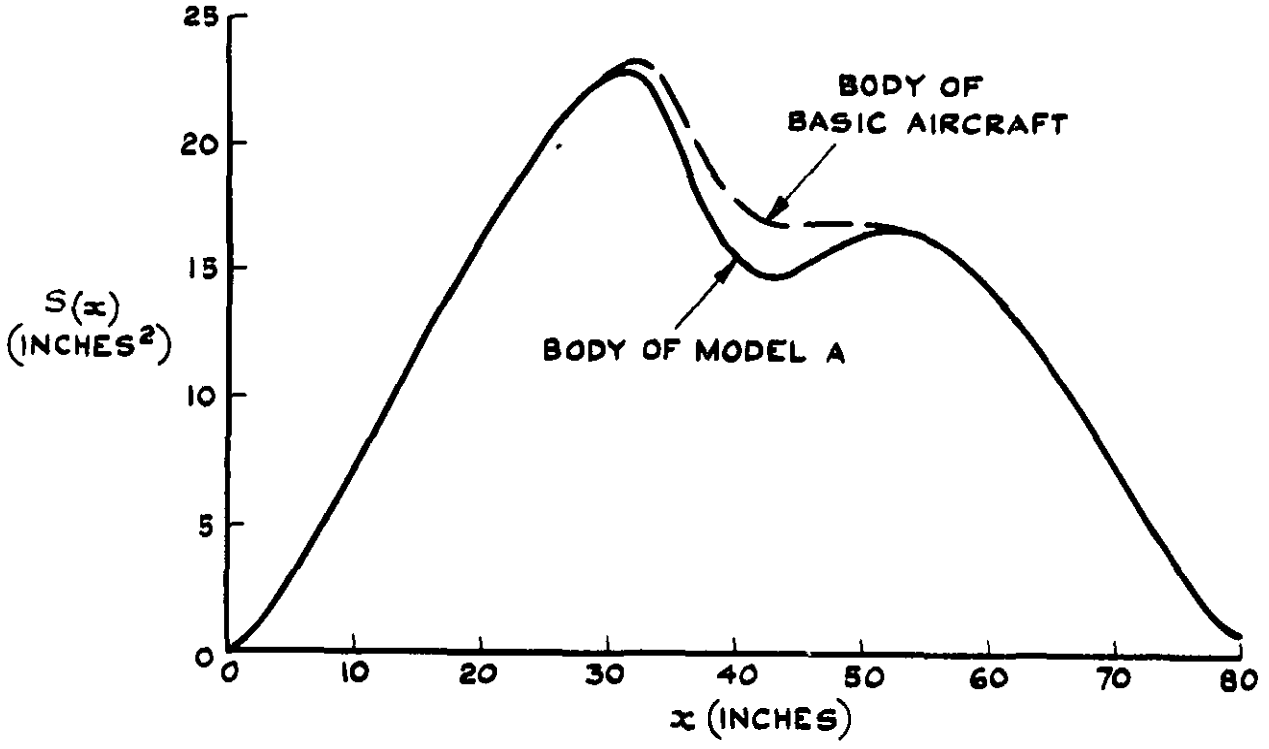

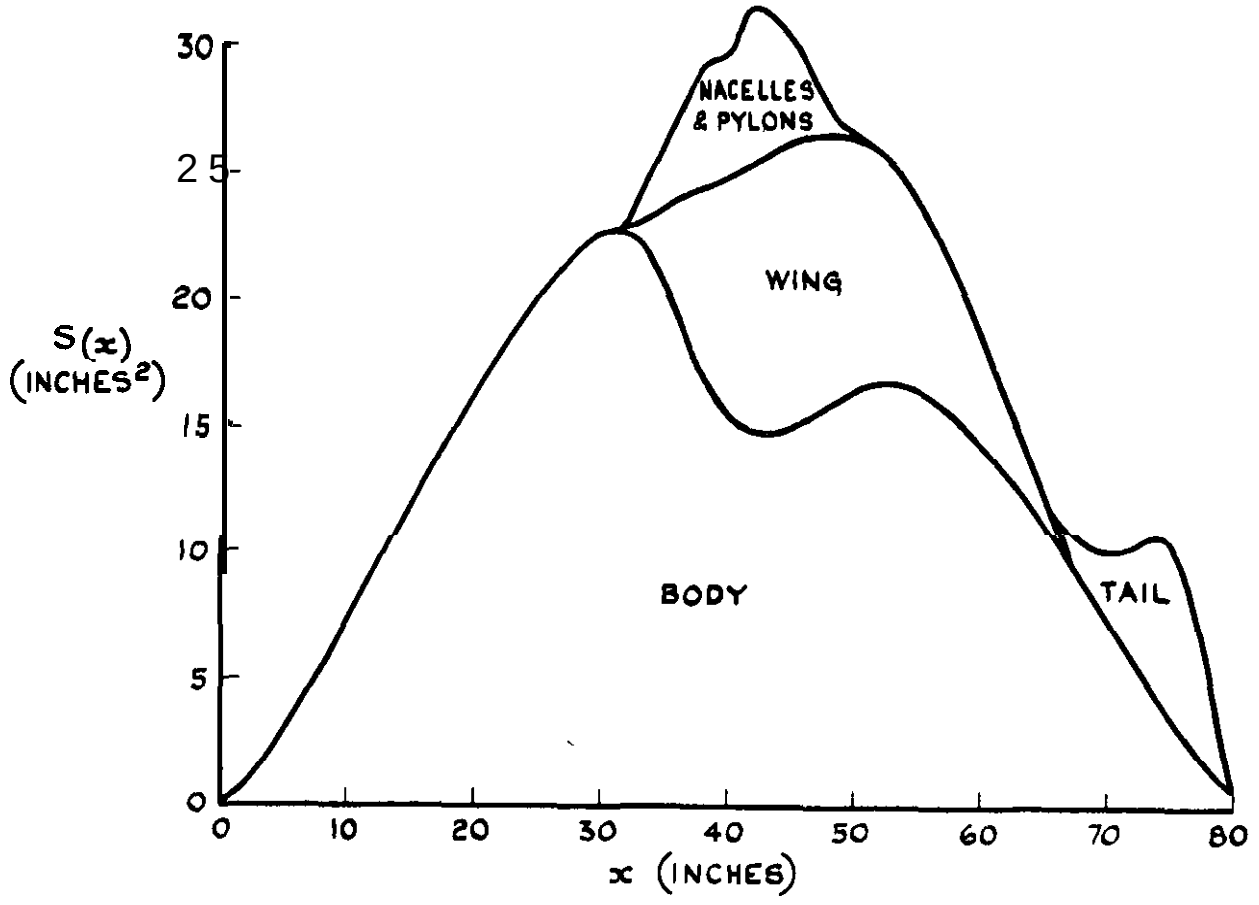

FIG. 8 (a) MODEL A

FIG. 8 NORMAL AREA DISTRIBUTION OF THE BODIES AND THE COMPLETE MODELS

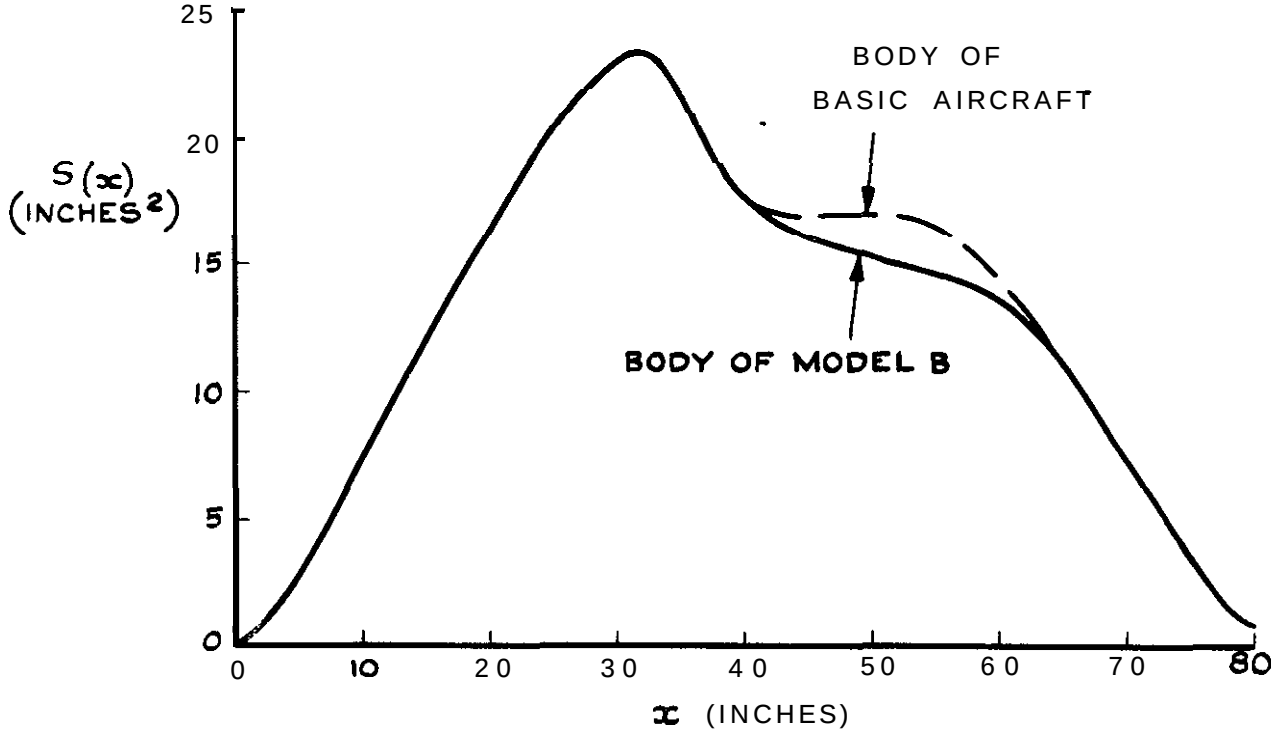

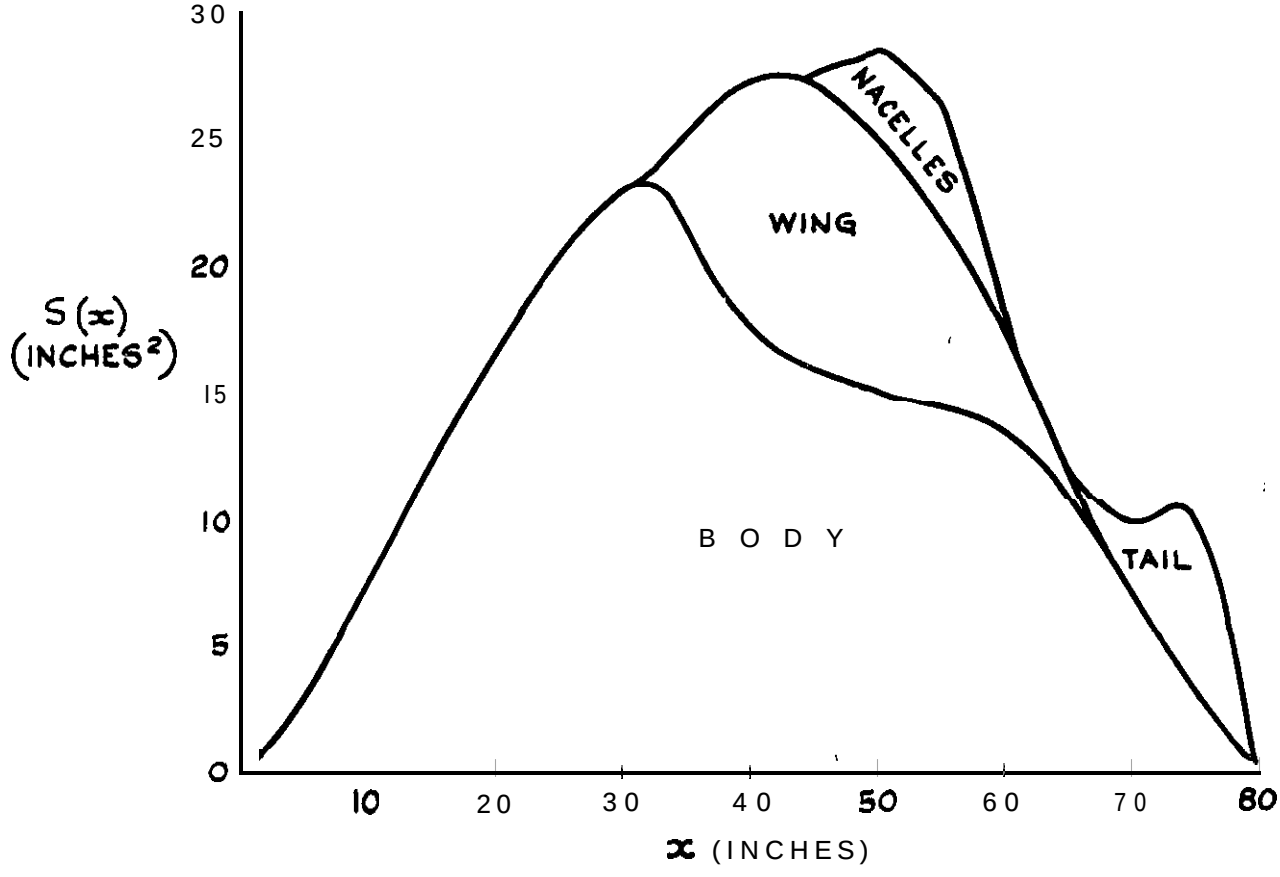

FIG 8 (b) MODEL B

FIG. 8 (CONTD)

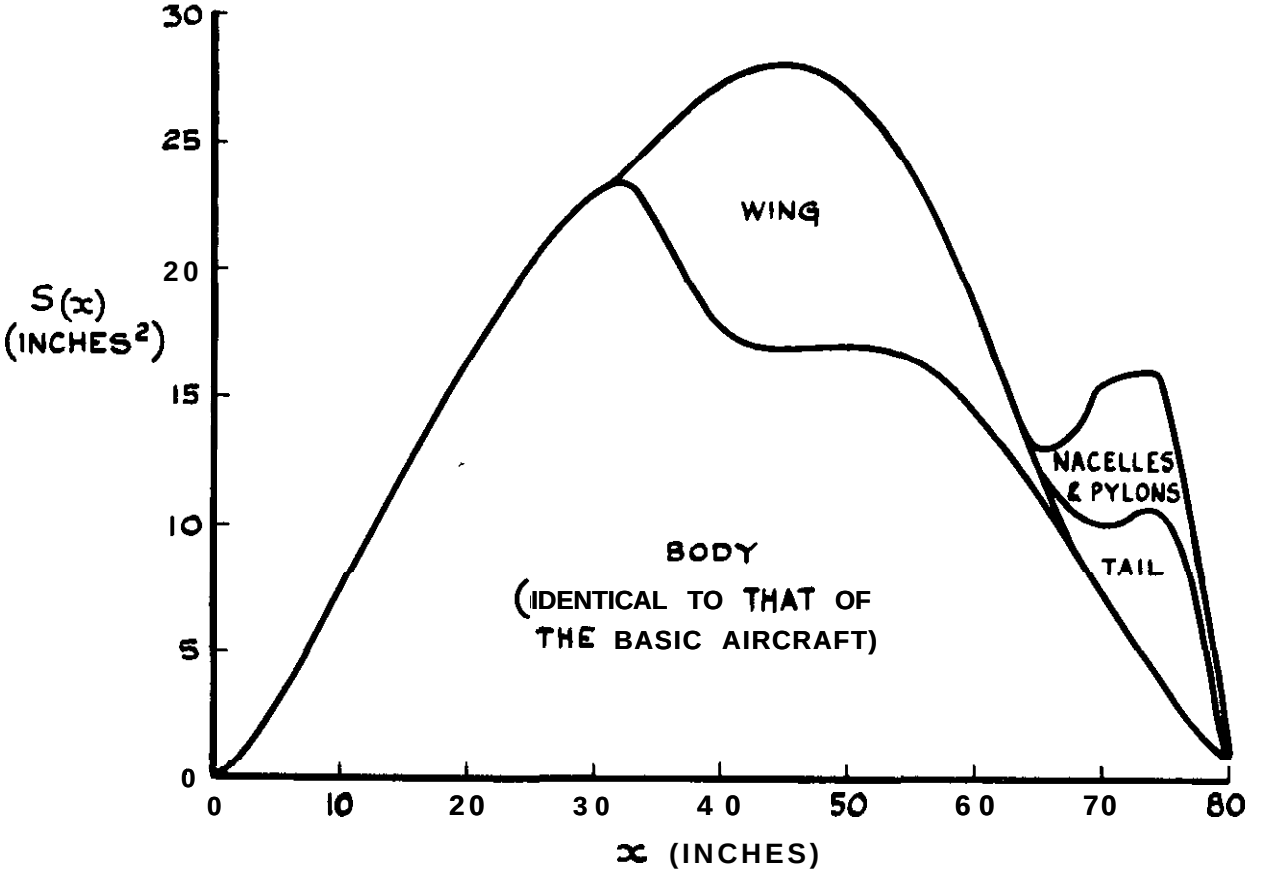

FIG. 8 (C) MODEL C

FIG. 8 (CONCLD)

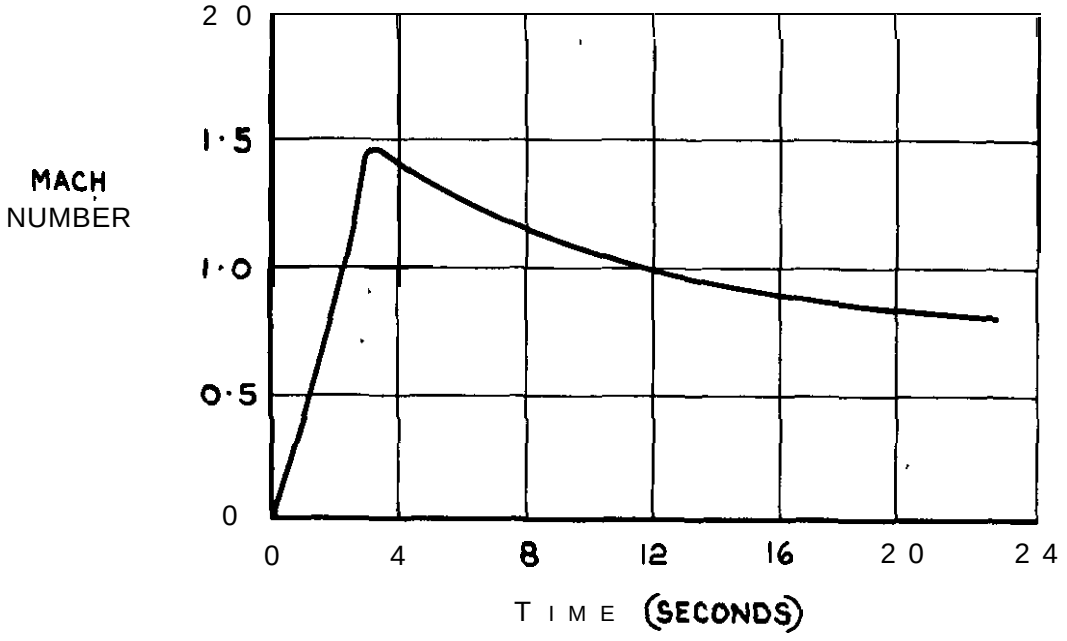

FIG.9 TYPICAL VARIATION OF MACH NUMBER WITH TIME (MODEL A)

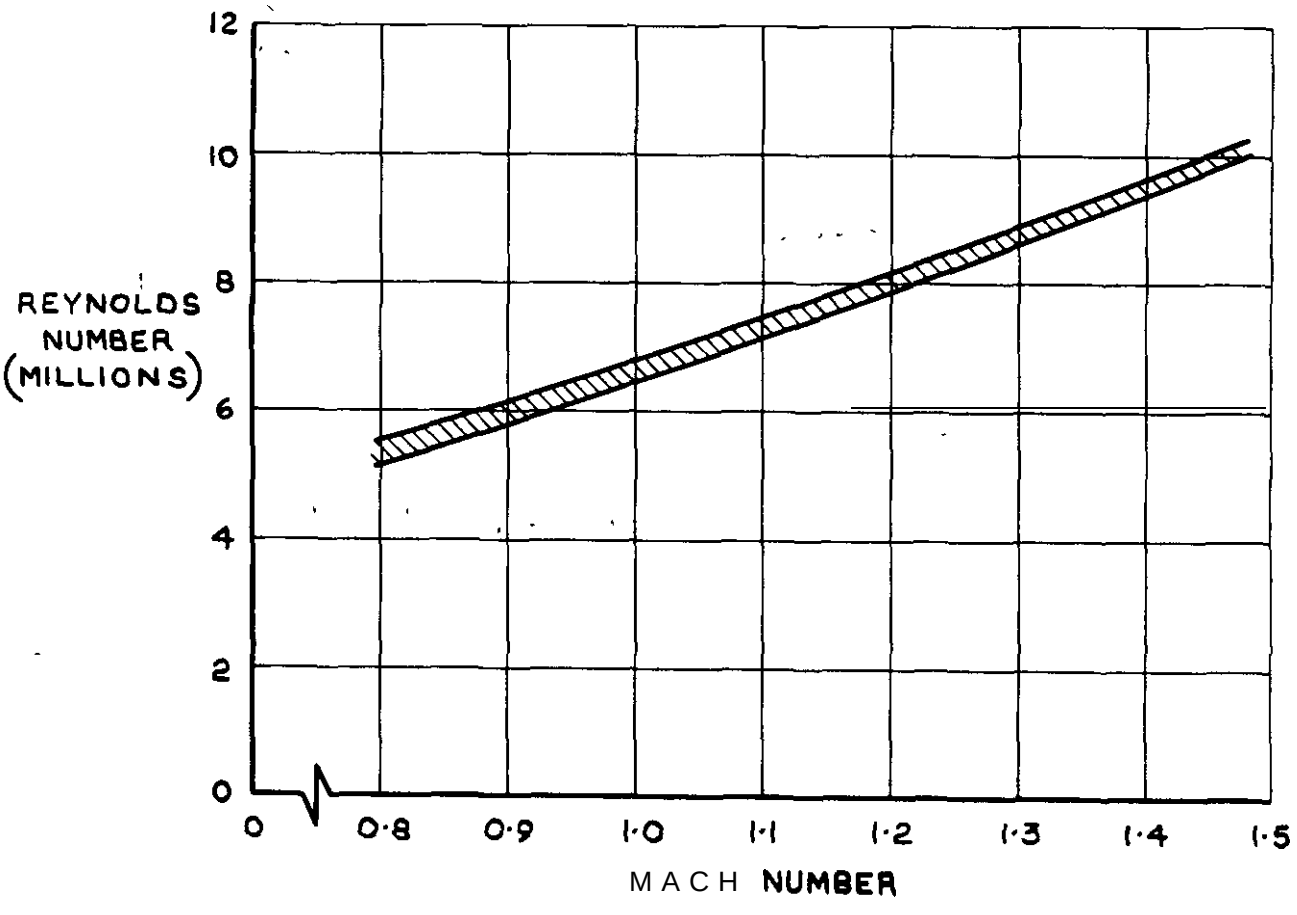

FIG. 10 REYNOLDS NUMBER

(BASED ON $\bar{c}$)

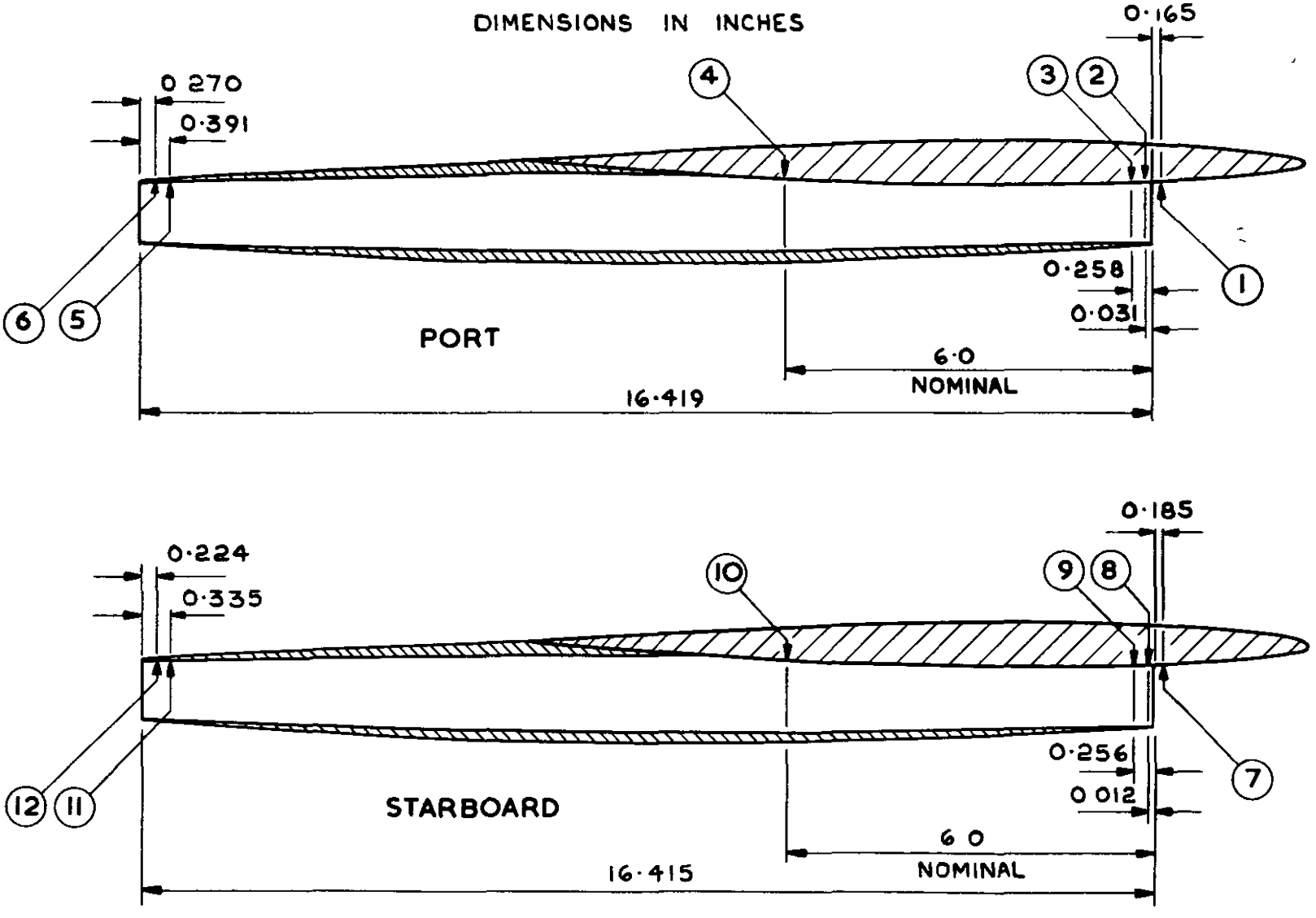

FIG.11 POINTS AT WHICH STATIC PRESSURE WAS MEASURED IN THE NACELLES OF MODEL B

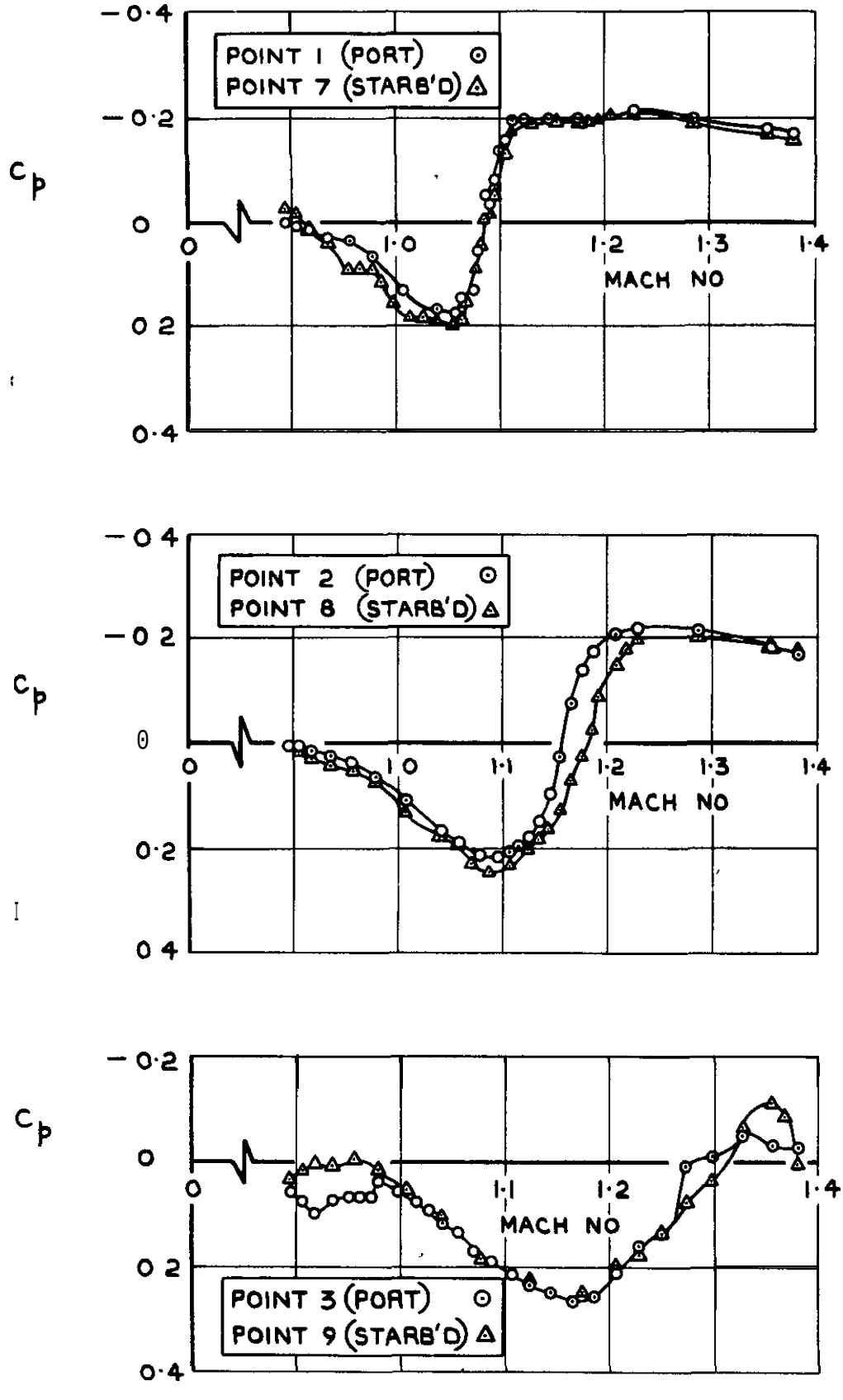

FIG.12 PRESSURES IN THE NACELLES OF MODEL B

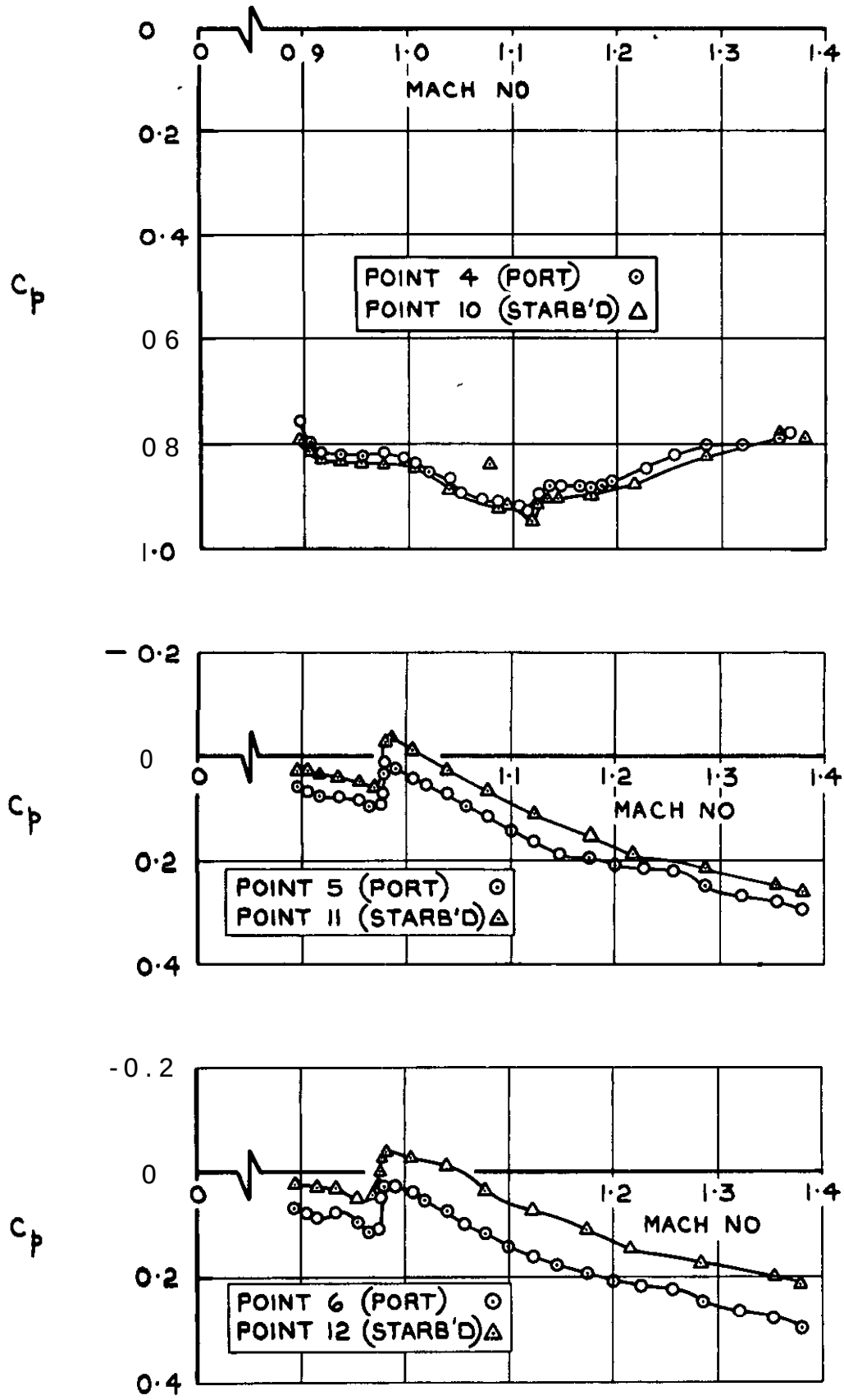
0
0·2
0·4
0·6
0·8
1·0
0·9
1·0
1·1
1·2
1·3
1·4
MACH NO
C_p
POINT 4 (PORT) ⊙
POINT 10 (STARB'D) △
−0·2
0
0·2
0·4
MACH NO
C_p
POINT 5 (PORT) ⊙
POINT 11 (STARB'D) △
-0.2
0
0·2
0·4
MACH NO
C_p
POINT 6 (PORT) ⊙
POINT 12 (STARB'D) △

FIG. 12 (CONTD)

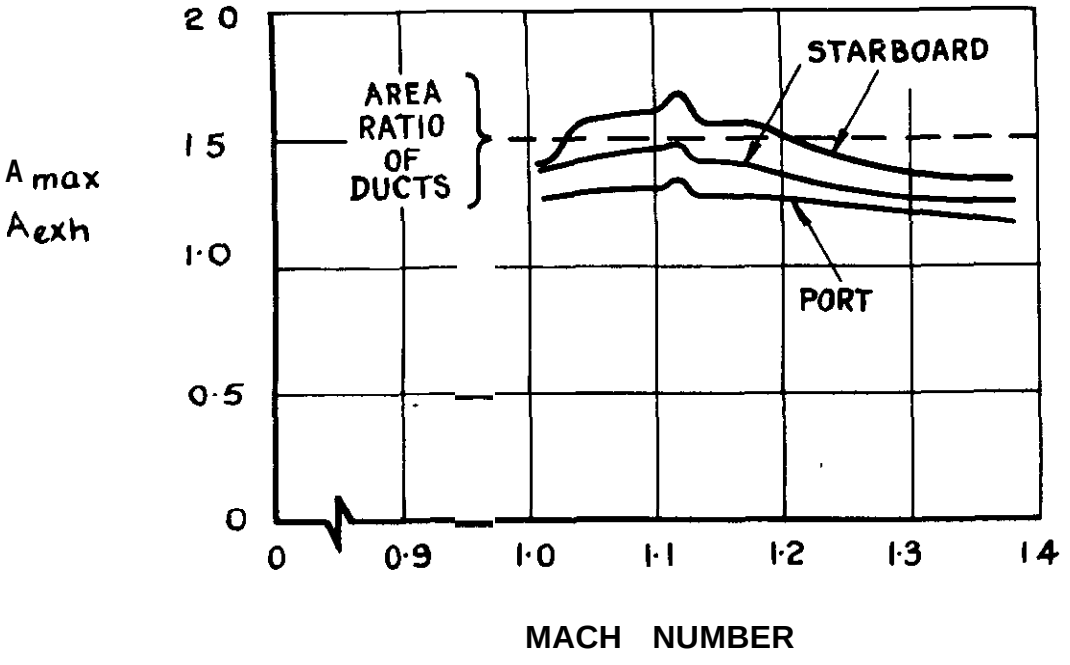

FIG. 13 EFFECTIVE INTERNAL CROSS-SECTION AREA RATIOS REQUIRED TO PRODUCE THE PRESSURE RATIOS MEASURED IN THE NACELLES OF MODEL B

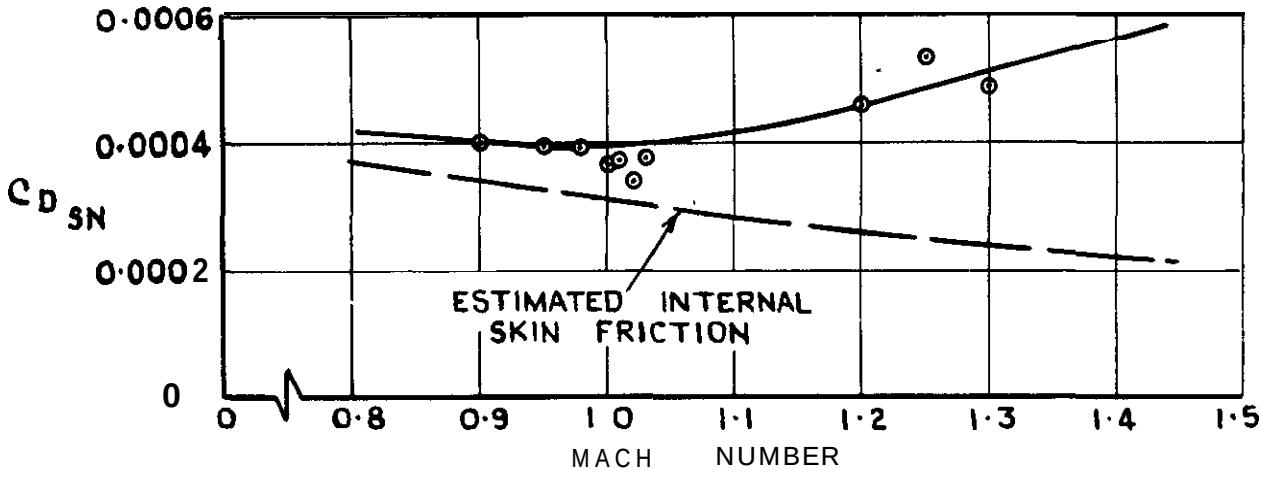

FIG. 14(a) STANDARD INTERNAL DRAG

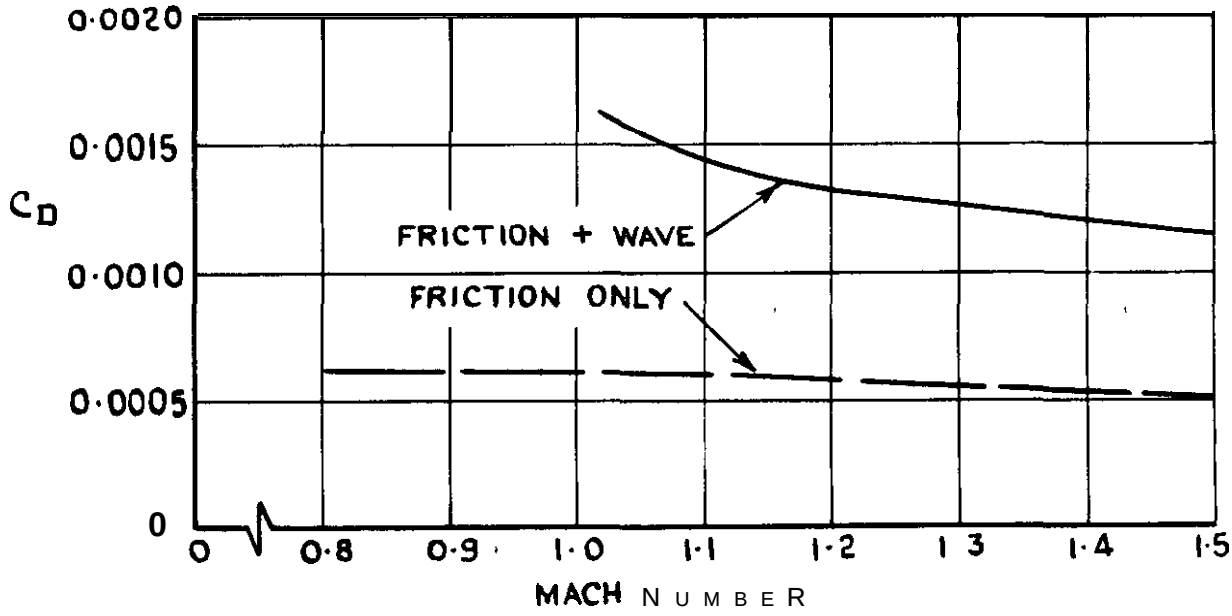

FIG.1 4 (b) ESTIMATED EXTERNAL DRAG

FIG. 14. DRAG OF ONE ISOLATED NACELLE

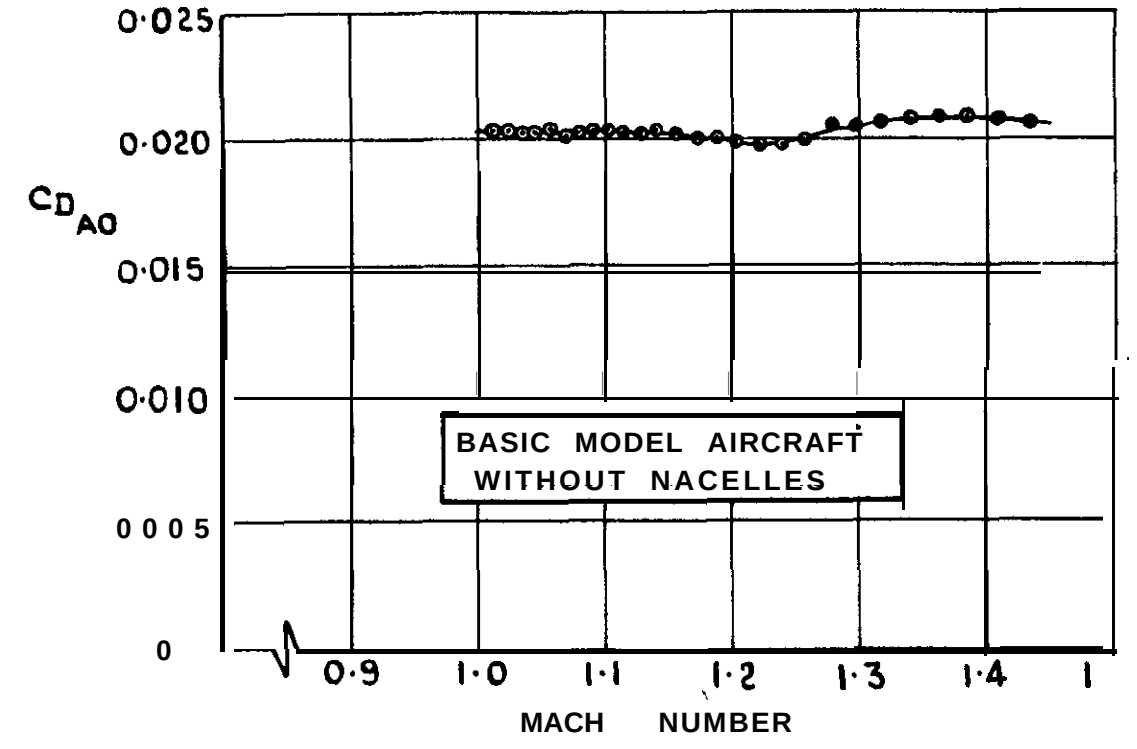

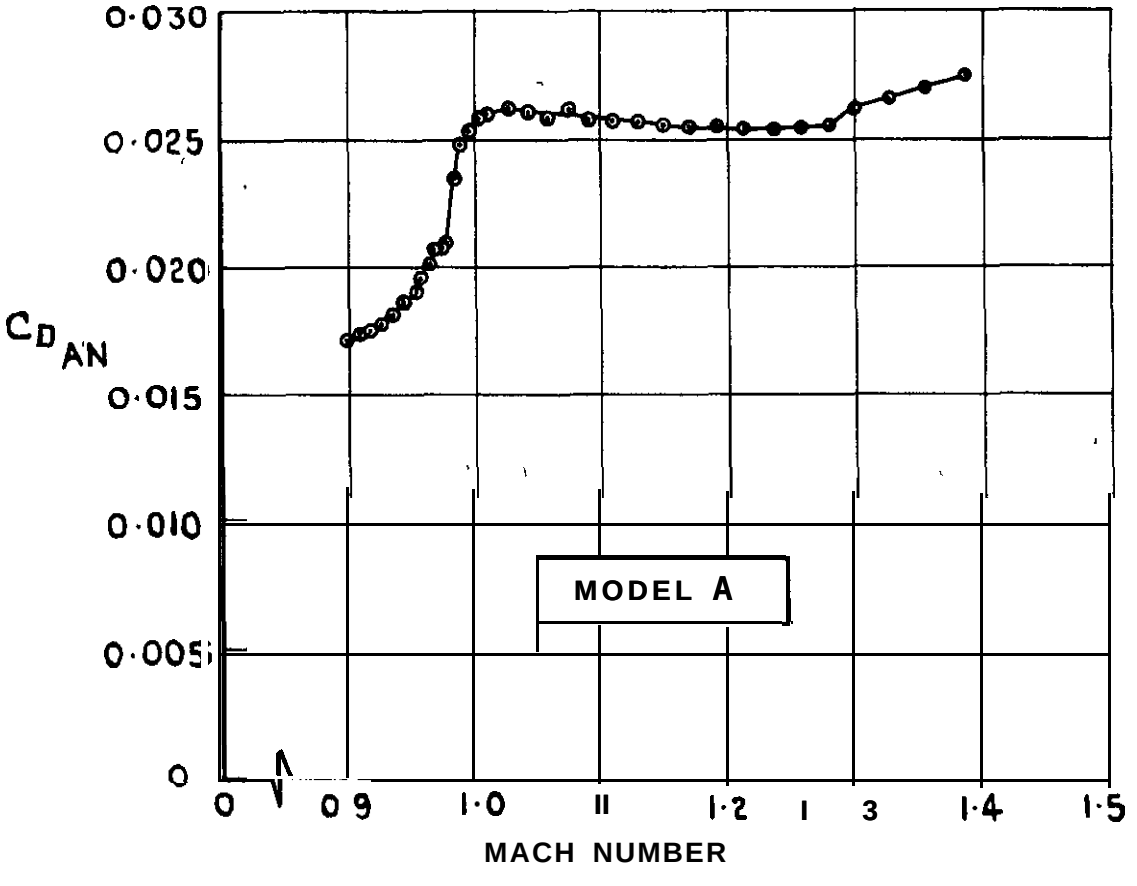

FIG. I5 TOTAL DRAG COEFFICIENT OF MODELS IN FLIGHT

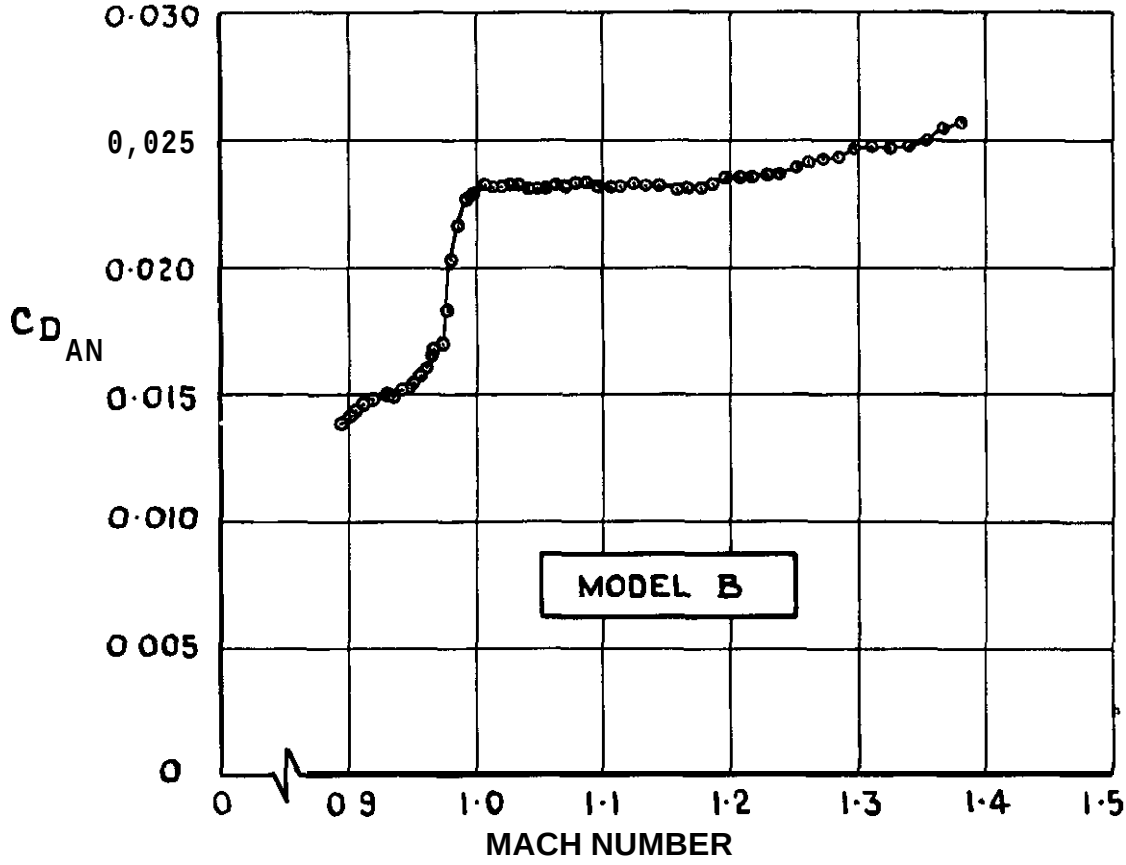
0·030
0,025
0·020
$C_{D_{AN}}$
0·015
0·010
0 005
0
0
0 9
1·0
1·1
1·2
1·3
1·4
1·5
MACH NUMBER
MODEL B

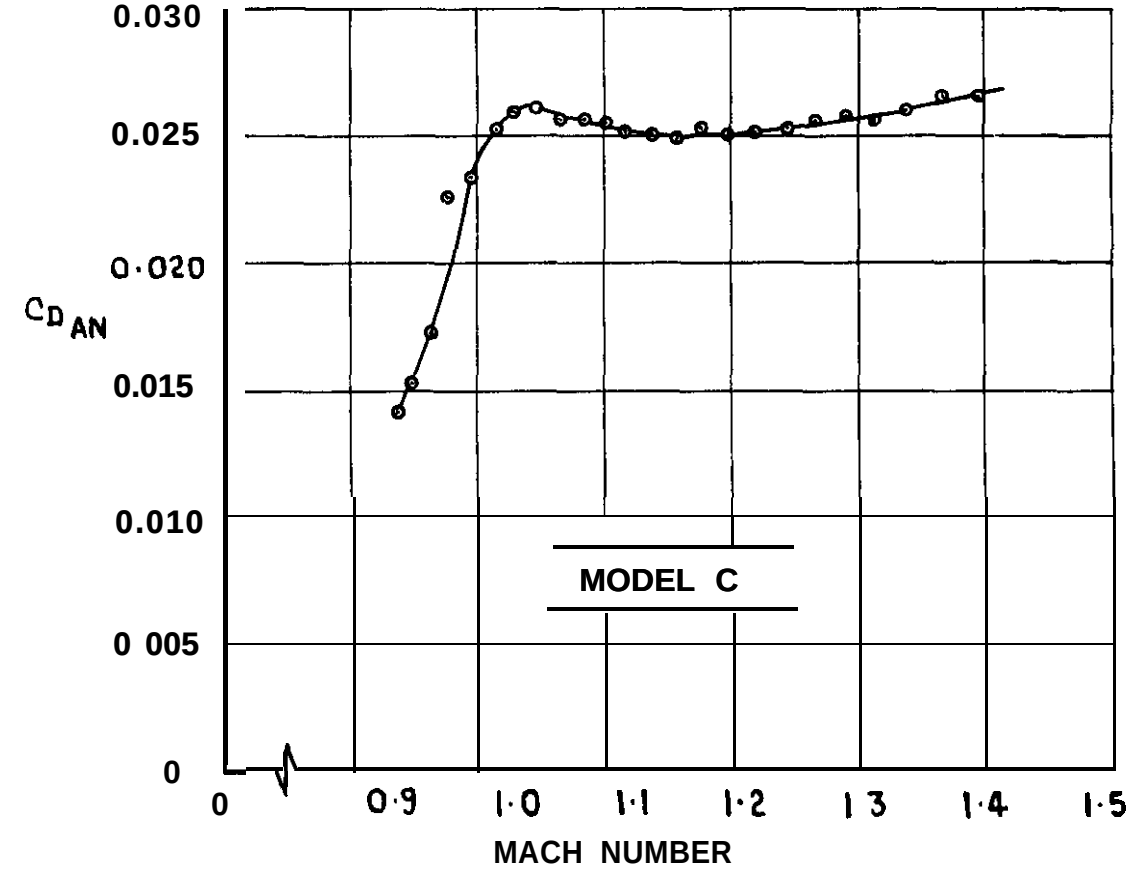
0.030
0.025
0·020
$C_{D_{AN}}$
0.015
0.010
0 005
0
0
0·9
1·0
1·1
1·2
1 3
1·4
1·5
MACH NUMBER
MODEL C

FIG. 15 (CONTD)

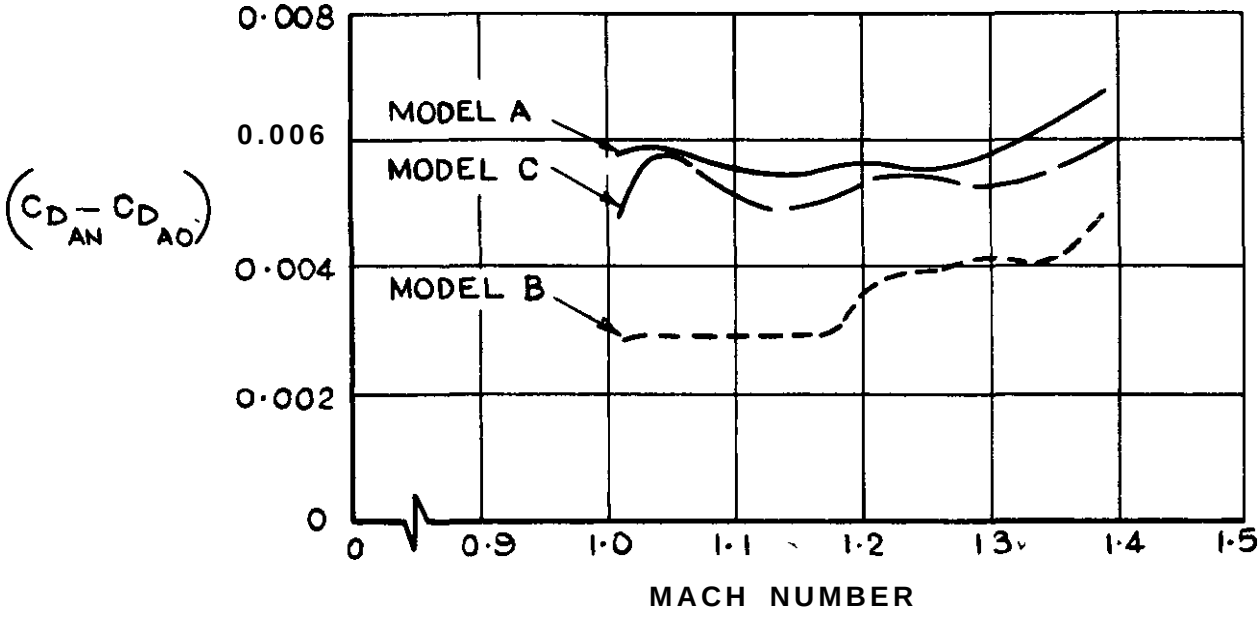

FIG. 16 TOTAL DRAG INCREMENT CAUSED BY NACELLE INSTALLATION

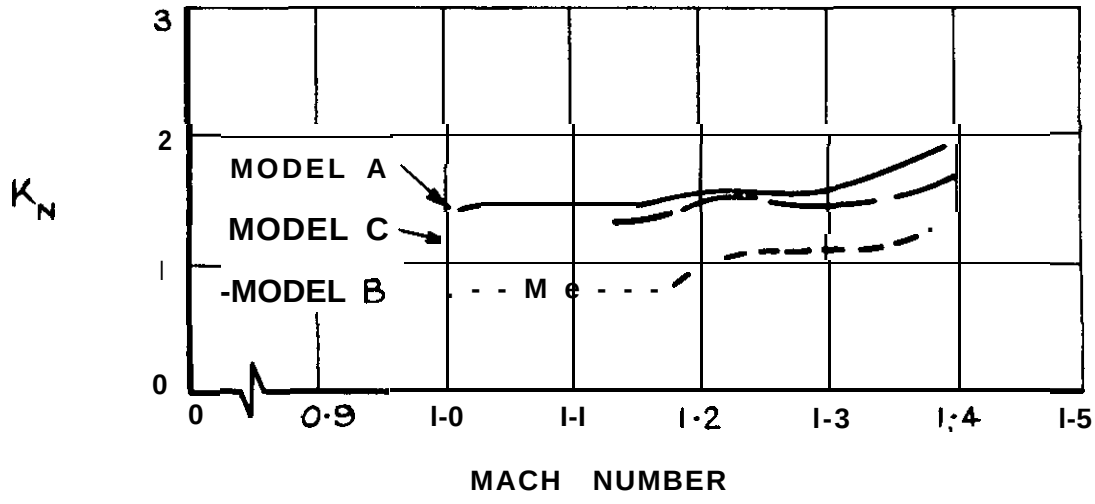

FIG. 17 RATIO OF THE TOTAL DRAG INCREMENT CAUSED BY NACELLE INSTALLATION TO THE DRAG OF TWO ISOLATED NACELLES

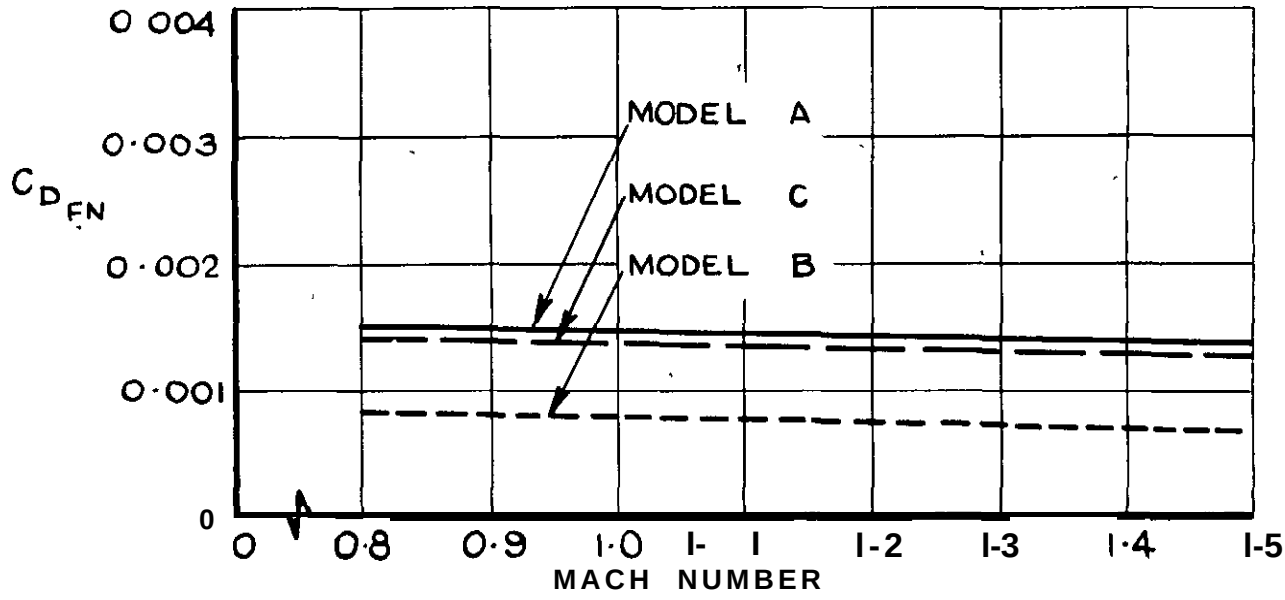

FIG. 18 ESTIMATED ADDITIONAL EXTERNAL SKIN-FRICTION DRAG CAUSED BY NACELLE INSTALLATION

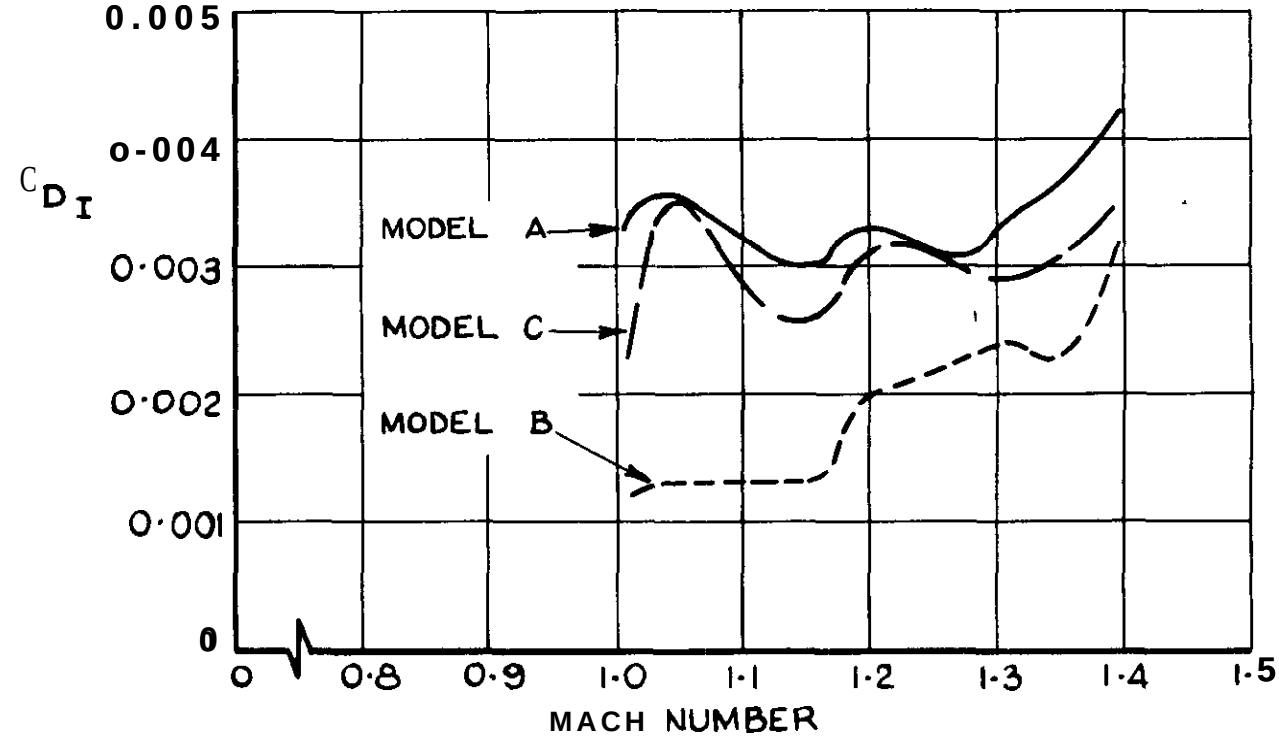

FIG. 19 INSTALLATION DRAG

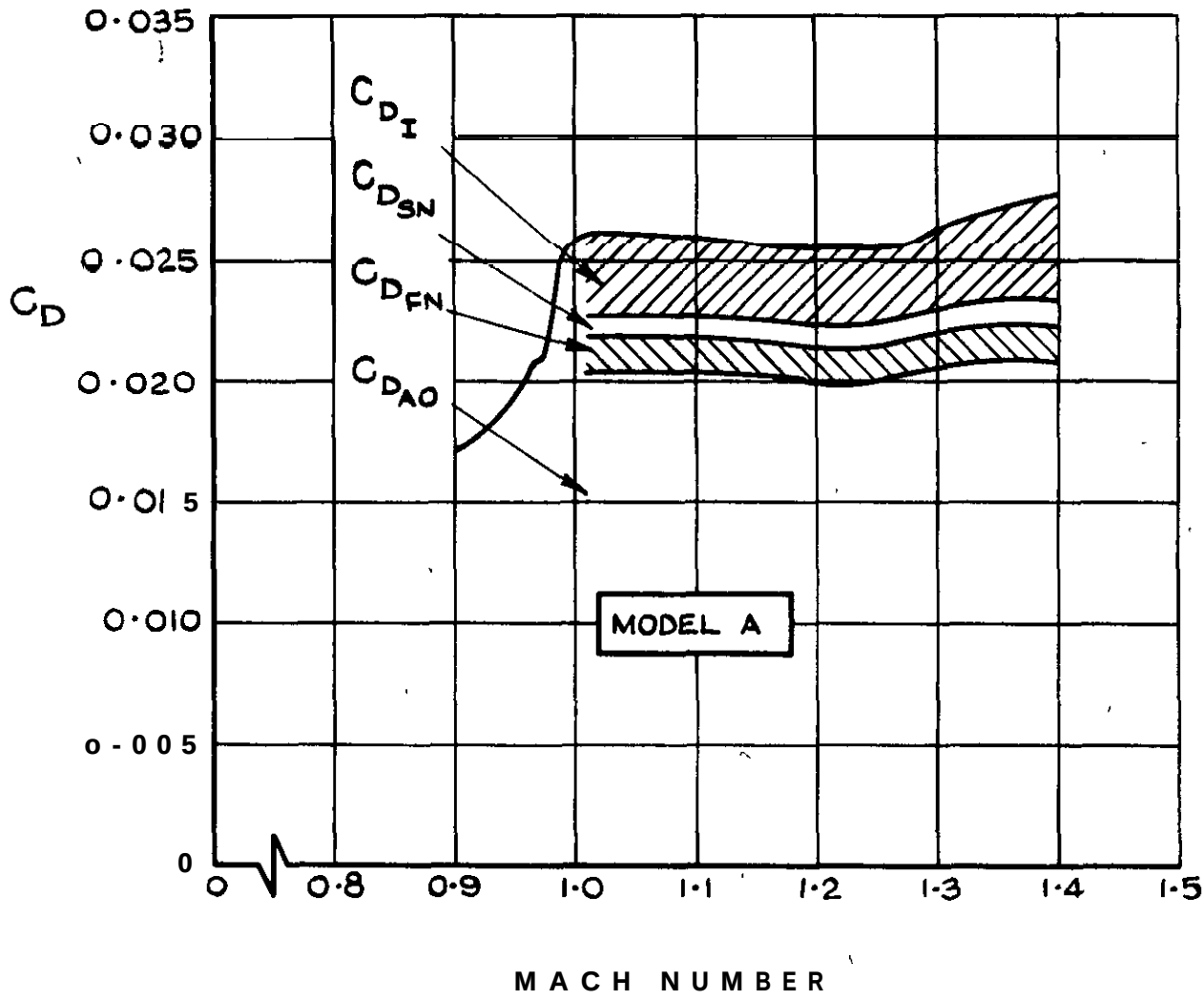

FIG. 20 DRAG BREAKDOWN

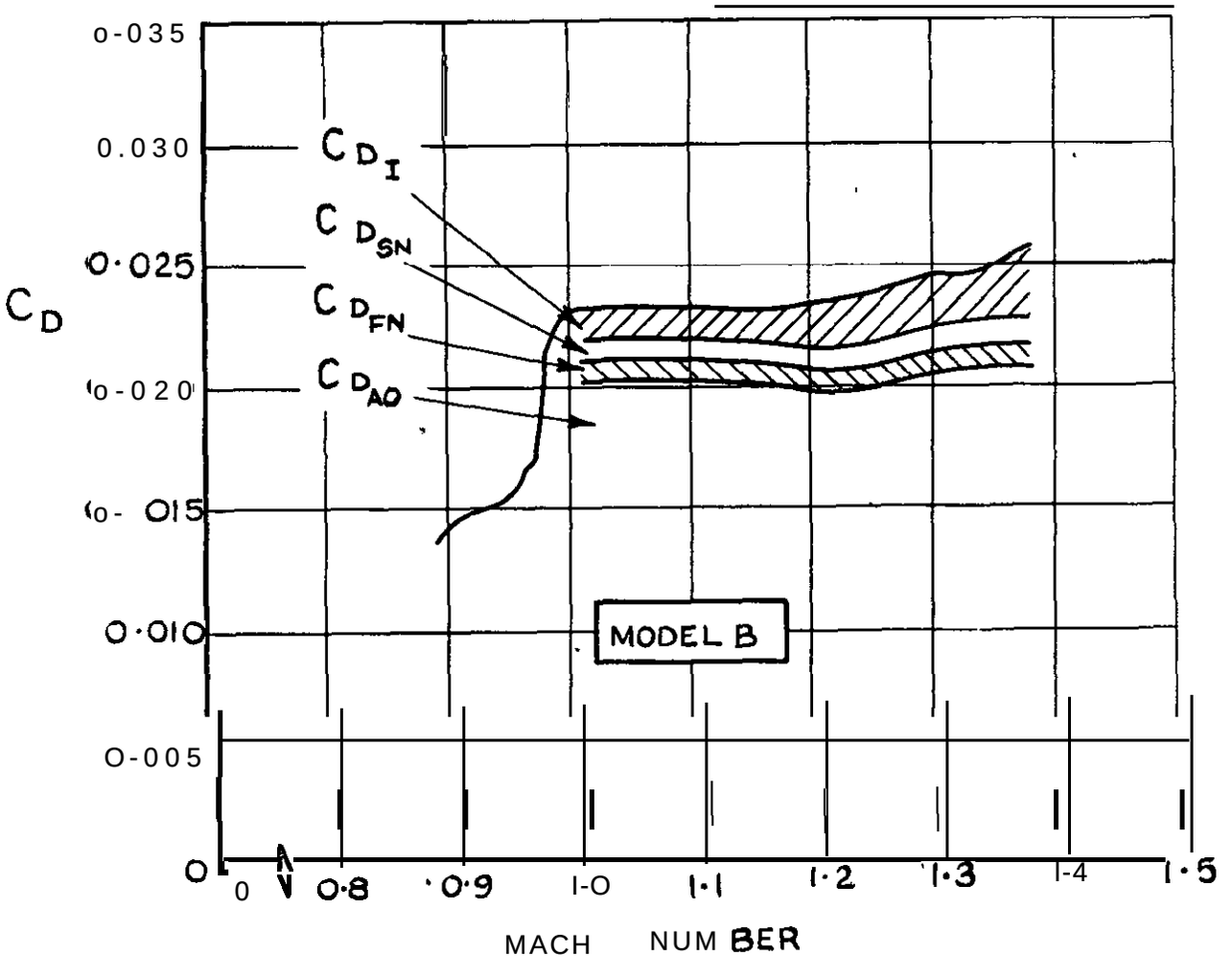
0-035
0.030
0·025
0-020
0- 015
0·010
0-005
0
C_D
C_{D_I}
$C_{D_{SN}}$
$C_{D_{FN}}$
$C_{D_{AO}}$
MODEL B
0
0·8
·0·9
I-O
1·1
1·2
1·3
I-4
1·5
MACH NUMBER

FIG. 20 (CONTD)

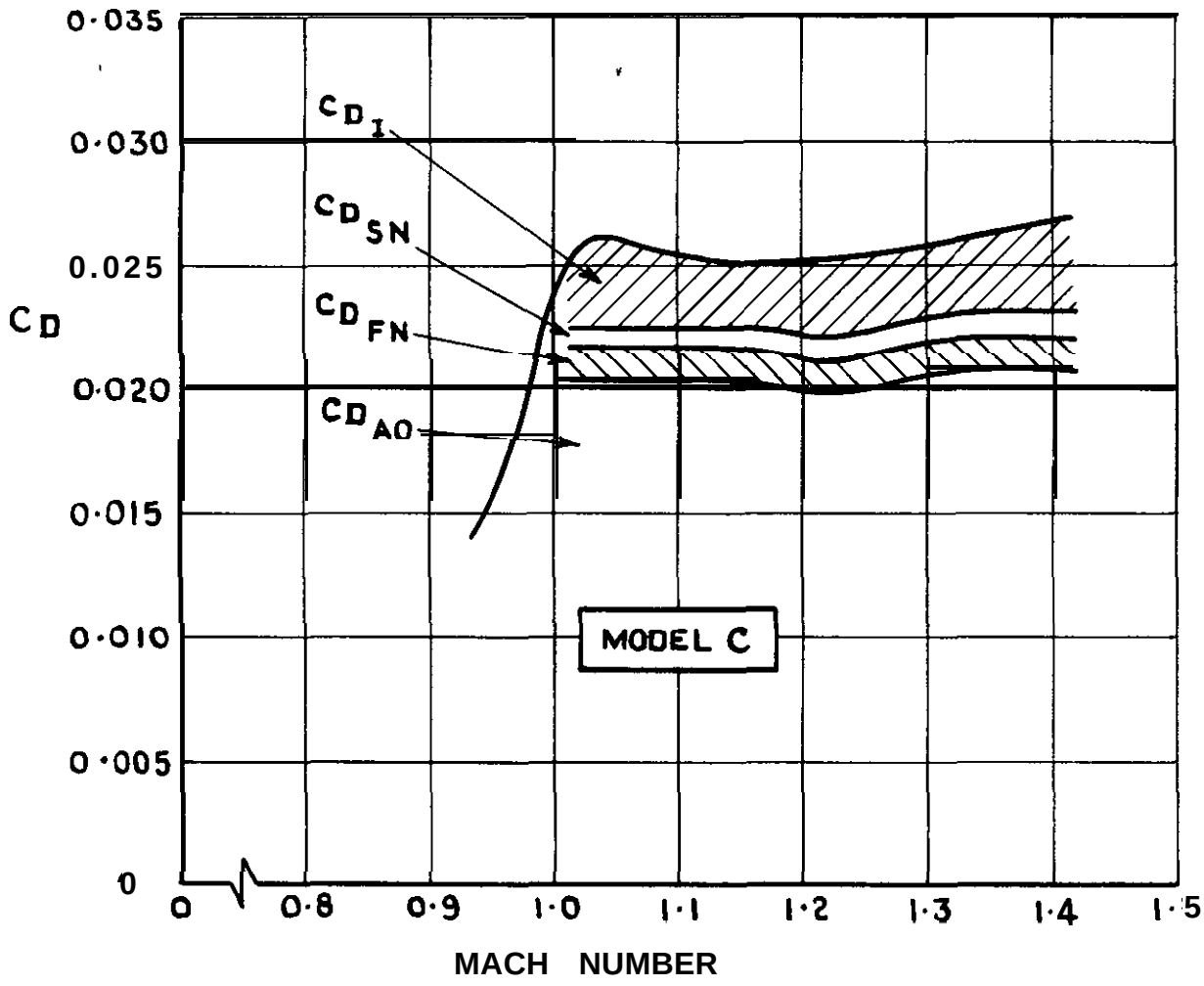

FIG. 20 (CONCLD)

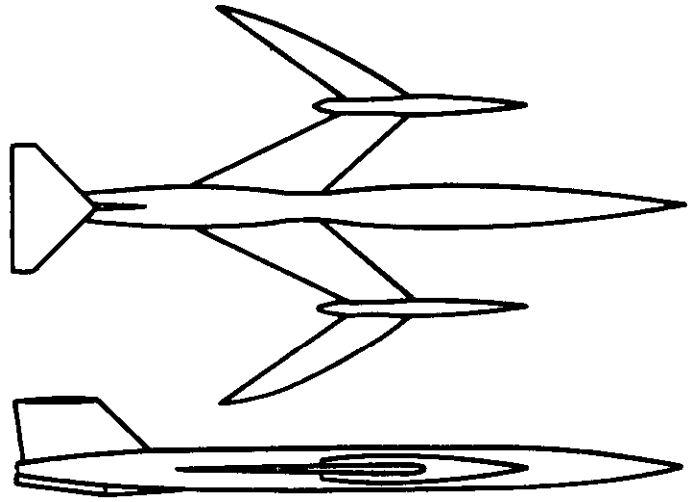

FIG.21 M-WING MODEL DERIVED FROM THE SWEPT-WING MODELS
(REFERENCE 10)

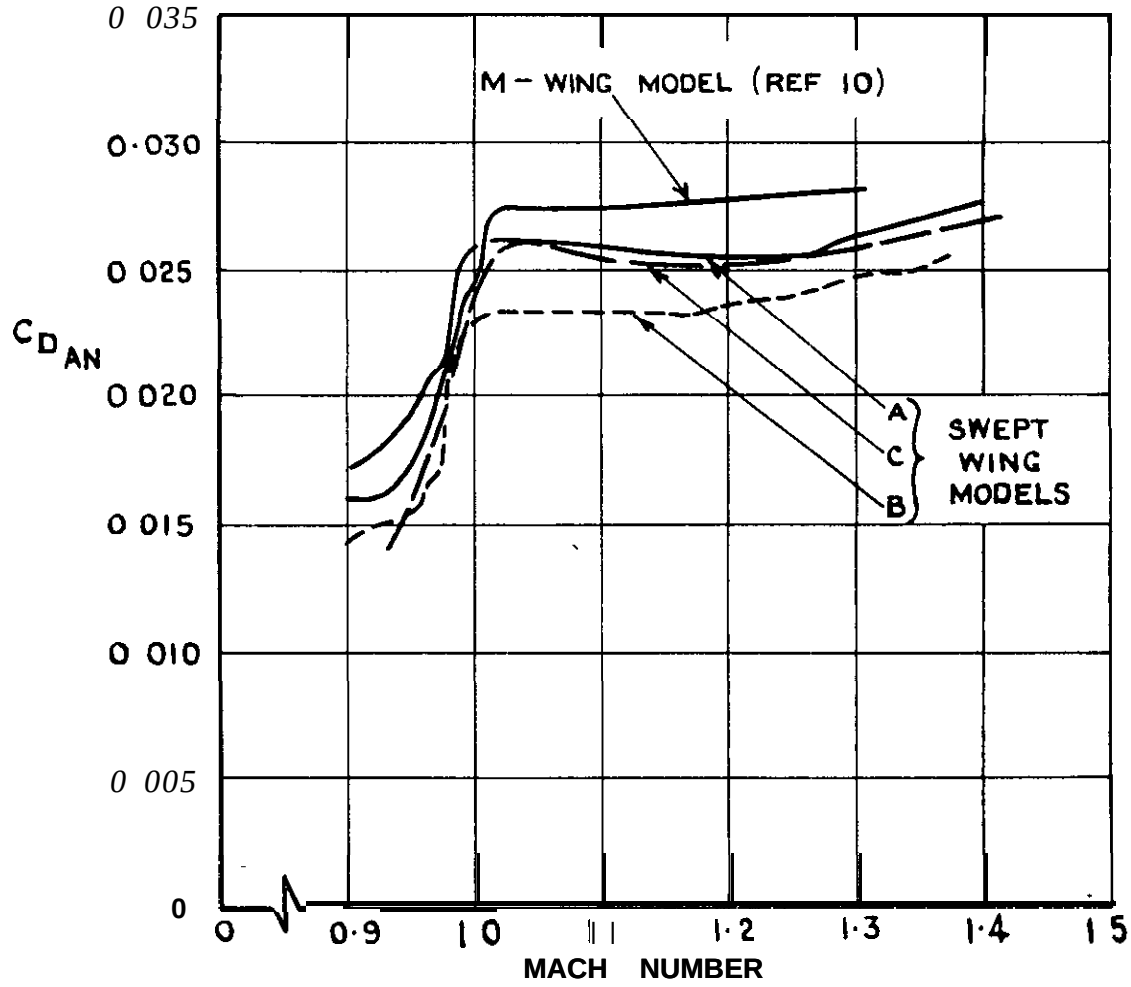

FIG. 22 DRAG COMPARISON BETWEEN SWEPT-WING AND M-WING MODELS WITH NACELLES

Printed in England for Her Majesty's Stationery Office by the Royal Aircraft Establishment, Farnborough. Dd.129528. K.4.

A.R.C. C.P.960
June 1966

533.6.013.12 : 53.695.9 : 533.695.129 : 533.6.011.35

Hunt, G.K.

FREE-FLIGHT MEASUREMENTS OF THE INCREMENTAL DRAG DUE TO ENGINE NACELLES ON A TRANSONIC SWEPT-WING AIRCRAFT

Models of a swept-wing aircraft, without nacelles and with a pair of simple nacelles attached in three different ways, were flown at transonic and low supersonic speeds at Reynolds numbers up to 10 million. From measurements of their zero-lift drag the incremental drag caused by each nacelle installation was determined.

A breakdown of the incremental drag shows that, at the design Mach number of 1.2. the external drag caused by a pair of pylon-mounted nacelles on the wing or on the body was about twice that caused by a pair of nacelles attached directly to the wing.

A.R.C. C.P.960
June 1966

53.6.013.12 : 533.695.9 : 533.695.129 : 53.6.011.35

Hunt, G.K.

FREE-FLIGHT MEASUREMENTS OF THE INCREMENTAL DRAG DUE TO ENGINE NACELLES ON A TRANSONIC SWEPT-WING AIRCRAFT

Models of a swept-wing aircraft, without nacelles and with a pair of simple nacelles attached in three different ways, were flown at transonic and low supersonic speeds at Reynolds numbers up to 10 million. From measurements of their zero-lift drag the incremental drag caused by each nacelle installation was determined.

A breakdown of the incremental drag shows that, at the design Mach number of 1.2, the external drag caused by a pair of pylon-mounted nacelles on the wing or on the body was about twice that caused by a pair of nacelles attached directly to the wing.

A.R.C. C.P.960
June 1966

53.6.013.12 : 533.695.9 : 533.695.129 : 53.6.011.35

Hunt, G.K.

FREE-FLIGHT MEASUREMENTS OF THE INCREMENTAL DRAG DUE TO ENGINE NACELLES ON A TRANSONIC SWEPT-WING AIRCRAFT

Models of a swept-wing aircraft, without nacelles and with a pair of simple nacelles attached in three different ways, were flown at transonic and low supersonic speeds at Reynolds numbers up to 10 million. From measurements of their zero-lift drag the incremental drag caused by each nacelle installation was determined.

A breakdown or the incremental drag shows that, at the design Mach number of 1.2. the external drag caused by a pair of pylon-mounted nacelles on the wing or on the body was about twice that caused by a pair of nacelles attached directly to the wing.

DETACHABLE ABSTRACT CARDS

Published by
HER MAJESTY'S STATIONERY OFFICE

To be purchased from
49 High Holborn, London W C 1
423 Oxford Street. London W 1
13.4 castle Street. Edinburgh 2
109 St Mary Street, Cardiff
Brazennose Street, Manchester 2
50 Fairfax Street, Bristol 1
35 Smallbrook, Ringway, Birmingham 5
7-11 Linenhall Street, Belfast 2
or through any bookseller

S.O. CODE No. 23-9017-60